Shallow, old and hydrologically insignificant fault zones in the Appalachian orogen

Juliette Malgrange, Civil Engineering and Applied Mechanics,
McGill University, Montréal

December, 2012

A thesis submitted to McGill University in partial fulfillment of the requirements of the degree of Master Engineering in Civil Engineering

Abstract

Understanding and quantifying fluid flow patterns and the permeability architecture of fault zones is crucial for petroleum development, the safety of nuclear waste repositories, and water resource management. Fault zones have complex permeability patterns that lead to faults acting as hydraulic barriers, conduits, or combined conduit-barriers. How faults affect groundwater flow at a regional scale (1-10km) is especially uncertain. The objective of this work is to determine whether faults affect regional patterns of groundwater discharge to lakes. We use naturally occurring geochemical tracers to quantify the groundwater discharge to lakes underlain by faults and not underlain by faults, and used groundwater discharge as a proxy for permeability. We sampled 54 lakes overlying the Paleozoic Appalachian fold and thrust belt in the Eastern Townships in Québec, and compared results to a previous study of lakes with low groundwater discharge in a crystalline watershed in the Canadian Shield not overlying regional fault zones. About half of the lakes sampled overly regional-scale thrust faults and the remaining lakes are not underlain by a fault. Lake water, inlet water and nearby groundwater were sampled in fall 2011 for radon-222 and chloride. Groundwater and surface water inflows have been quantified for each lake using a steady-state analytical mixing model of mass balance for both tracers, considering tracer input from precipitation, surface water and groundwater inflow, and loss through evaporation, gas exchange, radioactive decay, and surface water outflow. The uncertainty and physical plausibility of the analytical model results were examined using Monte Carlo analysis and numerical modeling, respectively. While the analytical model indicates non-negligible groundwater discharge for most of the lakes, the difference between the discharge rate into the lakes located on faults and the other lakes is not statistically significant. Numerical modeling suggests that fault zone permeability parameters are insignificant compared to watershed parameters such as lake or watershed area. However, the groundwater discharge rate in the Paleozoic fold-belt is significantly higher than lakes overlain crystalline bedrock. Thus, the rate of groundwater discharge is not significantly enhanced or diminished around the thrust fault zones, suggesting that in a regional scale, permeability of fault zones is not significantly different from the bedrock permeability at shallow depth in this old, tectonically-inactive sedimentary fold and thrust belt.

Résumé

L'étude de la perméabilité des zones de failles, et la caractérisation des écoulements souterrains autour des failles est un défi essentiel pour nombre de champs d'études, comme l'industrie pétrolière, l'enfouissement des déchets nucléaires, ou pour la gestion des ressources en eau. La perméabilité des zones de failles est complexe, et une faille peut se comporter aussi bien comme une barrière hydraulique que comme un conduit, ou encore une association des deux, favorisant les écoulements le long de la faille. L'impact des failles sur les écoulements souterrains est inconnu, en particulier à une échelle régionale (1-10km). L'objectif de notre étude est d'étudier l'effet des failles sur les écoulements souterrains régionaux, en particulier sur les échanges entre les eaux de surface et les eaux souterraines. L'étude porte sur 54 lacs des Cantons de l'Est (Québec), dont la moitié recouvre une zone de faille. Les lacs sont situés dans la zone de Dunnage dans les Appalaches, formée de roches du Paléozoïque inférieur. Le débit des eaux souterraines a été estimé pour chaque lac en utilisant un modèle stationnaire incluant des bilans de masse sur deux traceurs présents en grande quantité dans les nappes aussi bien que dans les eaux de surface : le radon-222 et les ions chlorures. Les résultats ont également été comparés à une étude réalisée auparavant sur des lacs à faible décharge souterraine situés dans le bouclier canadien et qui ne recouvrent pas de faille. L'incertitude du modèle, ainsi que sa pertinence physique ont été également évalués à l'aide respectivement d'analyses statistiques incluant des simulations de Monte Carlo, et d'une modélisation numérique. Alors que le modèle analytique donne des débits d'eaux souterraines importants pour presque tous les lacs, aucune différence significative n'a été observée entre les lacs situés sur une faille et les autres. Toutefois, les débits souterrains observés dans les roches sédimentaires et volcaniques des Appalaches sont de façon significative plus élevés que ceux observés dans le bouclier canadien. De la même façon, la modélisation numérique suggère que la perméabilité au sein de la zone de faille ne modifie pas notablement les débits souterrains, comparativement à des paramètres lies à la géométrie du bassin versant, comme la surface du bassin versant. Il en ressort que le débit souterrain ne semble pas notablement accentué en présence de faille, et ainsi, la perméabilité des failles, a une échelle régionale, ne diffère pas significativement de la perméabilité des roches environnantes, pour des aquifères peu profonds, dans cette ceinture.

Acknowledgements

I would like first to thank my supervisor Tom Gleeson who offered me a great project and was a great help and support throughout my thesis. I really appreciated it. I am also very thankful to Marie Larocque who let me run the radon analysis at her hydrogeology lab at UQAM, and to Sylvain who was a great assistance, and was such a pleasure to work with. Thanks a lot as well to Jeff McKenzie who let me use the IC in his lab in the Earth Science department at McGill, and Michael who considerably helped me with it. Thanks also to Luc Chouinard who was a great help to me for the statistics analysis.

Also, I address many thanks to the Elco, Claire and Elizabeth for their technical support, and their excellent advice.

I also want to thank all my friends who helped me during my project, and especially to the ones that came along with me for the field trips, and helped me collecting the samples, finding our way in the forests, and surviving hazardous entry in an asbestos mine: Zach, Elyes, Che, Amin, Hani, Amir, Alison, Doudou, Eva, Nataly, Kana, Luis.

Finally, I am also very thankful to all the people I met in the Eastern Townships, when I was collecting the samples, who let me take samples from their well, or from their docks, offered me to borrow their embarkation, and were very enthusiastic about the project, willing to share their experiences.

Contents

I. Introduction

Characterizing fault zones and understanding how they affect groundwater flow are essential to major engineering issues, such as nuclear water repositories, shale gas development, or contamination from mining or other industrial activities. Faults zones typically have high fracture densities and their permeability is heterogeneous and significantly different than the surrounding less deformed bedrock. Therefore the impact of fault zones on groundwater flow is important yet the impact depends on many parameters such as lithology, fault zone geometry, minor fractures patterns and connectivity, deformation conditions, fluid-rock interaction, and stress state. Fault zone permeability has been studied extensively at a local scale (1-100m) but very few field-based studies focus on faults impact at a regional scale (1-10 km). Although the effect of fault zones on local groundwater flow can be significant, we would investigate whether fault zones systematically affect regional groundwater flow significantly. We estimate groundwater discharge in order to characterize how fault zones affect permeability at a regional scale.

The objective of this study is to assess whether tectonically-inactive fault zones impact the groundwater discharge rates to overlying lakes. Groundwater discharge was quantified for 54 lakes in Eastern Quebec, using a mixing model of natural-occurring tracers, radon (^{222}Rn) and chloride. We sampled 21 lakes overlying thrust faults in the Appalachian Mountains in the Eastern Townships, and Chaudière-Appalaches, east of Montréal, Québec as well as 33 lakes not underlain by a fault zone (Figure 3), and compared the estimated discharge rates for both cases. We also compared results to similar results computed by Gleeson (2009) who used the same methodology to estimate groundwater discharge rates to lakes underlain by crystalline rock in the Canadian Shield which permeability is lower than in the sedimentary and volcanic rocks of the Appalachian Mountains. Darcy's law indicates that differences in groundwater discharge are due to differences in hydraulic gradient or permeability. In these humid regions the water table is generally near the surface (Winter, 1999; Winter et al., 1998) and the topographic gradients are generally consistent, suggesting differences in groundwater discharge would most likely be due to differences in permeability. Therefore, by comparing groundwater discharge to lakes located on a fault zones and to lakes away from any fault zones, we can assess whether fault zones significantly affect the regional subsurface hydrology due to their difference in permeability relative to the surrounding bedrock. The uncertainty of the model due to measurements errors or inaccuracy in parameters estimations was investigated using Monte Carlo simulations. In addition simulations of groundwater flow in faulted bedrock were carried out using the SUTRA numerical model. We simulated the groundwater discharge rates to lakes overlying fault zones. Observing the variations of the discharge rate with the changes on the fault zone characteristics and watershed dimensions we can understand how fault zones affect regional groundwater flow.

II. Literature review

Understanding and quantifying fluid flow patterns in fractured rock aquifers is a major challenge for numerous environmental engineering issues such as soil contamination and remediation, CO_2 sequestration, shale gas development, or nuclear waste repositories. Although fault zones have been widely studied and many conceptual models have been developed for different geological settings, fault zone permeability structure is generally poorly constrained, especially at a regional scale (1-10 kms). The impact of faults on regional groundwater systems (1-10s km) has been indeed examined by some studies (Flint et al., 2001; Saffer et al., 2003) but most structural and hydrogeological studies focus on the local scale (1-100s m).

Fault zone permeability structure depends on many parameters, such as lithology, fault displacement, 3-D fault zone geometry, deformation conditions, fluid-rock interaction, stress state, and fracture patterns and connectivity. Subsurface data is necessary to characterize 3-D permeability structure. Both structural geologists and hydrogeologists aim to characterize fault zones, using differing methods. Structural geologists investigate outcrops and analyze rock samples to design discrete fracture network models that describe fault zone permeability structure. Hydrogeologists collect detailed hydrogeological evidence from wells and springs in combination with geochemical surveys or groundwater temperature to trace groundwater flow paths. We describe both approaches, and include discrete fractures studies, although it is important to note that fractures are different than fault zones in that fractures do not have displacement.

Groundwater flow has also been studied through characterization of its interaction with surface water, using groundwater tracers, temperature or stable isotopes analysis. We also describe these methods since we apply them to estimate groundwater flow around fault zones for the first time.

a. Fault zone hydrology

The permeability of fault zones is complex, heterogeneous and difficult to predict *a priori* or without detailed study. Depending on the type, age, lithology, geometry and geologic history of the fault zone, they may act as conduits, barriers, or combined conduit-barrier systems that enhance or impede fluid flow (Aydin, 2000; Caine et al., 1996; Knipe, 1993).

Fault zones are often described as composed of two distinct components: a fault core, a zone of high strain where most of the displacement is accommodated, flanked by a damage zone of lesser strain, that is mechanically related to the growth of the fault zone (Figure 1;Caine et al., 1996; Chester and Logan, 1986; Evans et al., 1997). The fault zone is surrounded by relatively undeformed protolith or host rock. The two fault components have different hydraulic properties and there is no scalar relationship between them. The fault core is the central structure of the fault zone. It may include single slip surfaces (Caine et al., 1991a), unconsolidated clay-rich gouge zones (Anderson et al., 1983), brecciated and geochemically altered zones (Sibson, 1977) or highly indurated, cataclasite zones (Chester and Logan 1986). The reduction of grain size in the fault core leads to a reduction of porosity and permeability. The damage zone includes various fault related subsidiary structures that include small faults, veins, fractures, cleavage and folds that cause heterogeneity and anisotropy in the permeability structure and elastic properties of the fault zone (Bruhn et al., 1994). The fracture network controls the damage zone permeability and the high density of fractures typically makes it more permeable than the adjacent protolith. For instance, the damage zone permeability in the Dixie Valley fault zone is two to three orders of magnitude higher than the permeability of fractured protolith, and four to six orders of magnitude higher than the fault core permeability (Bruhn, 1993).

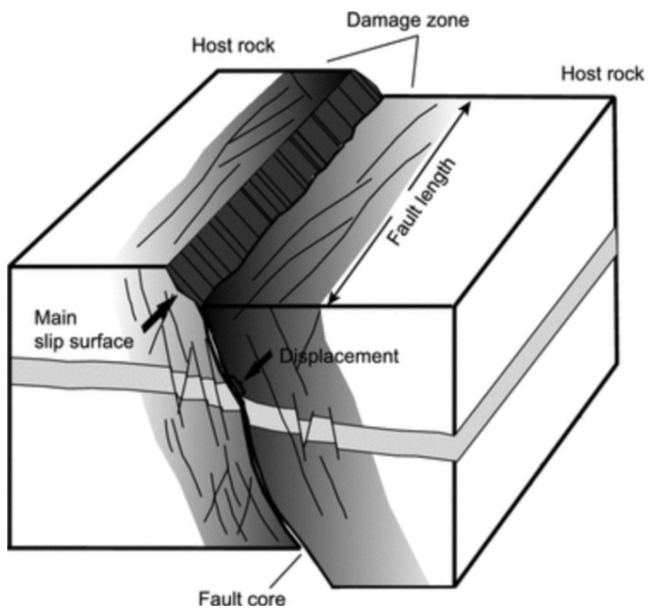

Figure 1: Conceptual model of fault zone (from Kolyukhin and Torabi., 2011)

The relative thickness of the fault core and the damage zones controls the overall permeability structure of a fault zone. Based on this idea, Caine et al. (1996) developed a conceptual scheme for fault related fluid flow in upper-crustal, brittle fault zones, represented on Figure 2. Four categories of fault zone permeability structure are associated with the relative width of fault components. When the damage zone is reduced in width, a fault will act either as a localized conduit, when the fault core is narrow or as a localized barrier when the fault core is wide. As the relative width of the damage zone expands, the fault can act as a distributed conduit if the fault core is insignificant. When the damage zone and the fault core are significant, the fault zone can act as a combined conduit-barrier with enhanced fault-parallel permeability and reduced fault-perpendicular permeability. For instance, small discrete fractures are seen as localized conduits in Shawangunk Mountains of eastern New York (Caine et al., 1991b), or deformation bands in sandstones that do not have a developed damage zone form a localized barrier to groundwater flow (Antonelli and Aydin, 1994). Depending on the permeability structure, different flow models should be used to estimate groundwater flow. For instance an equivalent porous medium can be used to study a distributed conduit, but for a localized conduit, the discrete fractures should be modeled as single conduits with parallel walls. A recent review of structural and hydrological data suggested that combined conduit-barrier are often the most common (Bense et al., submitted).

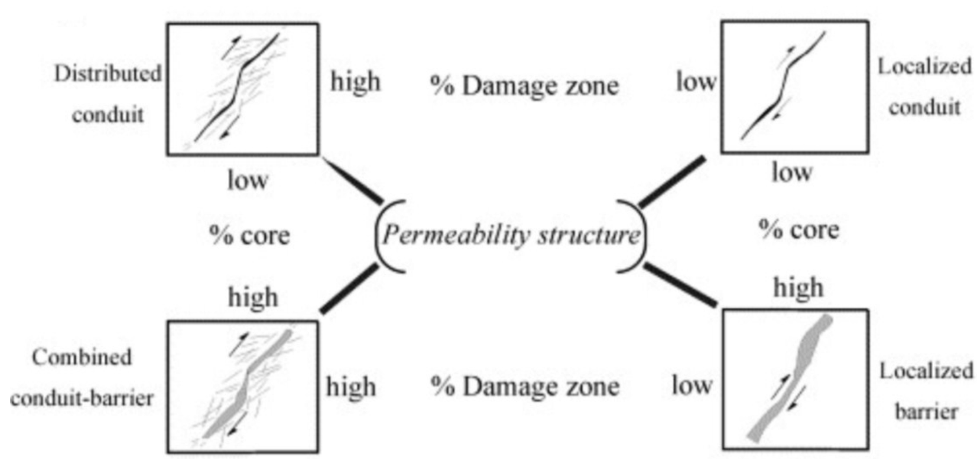

Figure 2. Conceptual scheme for fault-related fluid flow (from Caine et al., 1996)

The fault zone conceptual model by Caine et al (1996) does not apply in large-displacements faults in poorly-lithified sediments (Mozley and Goodwin, 1995). Poorly-lithified sediments do not macroscopically fracture, so the main element of the fault is the deformation band. Then a new fault-zone architecture element – the mixed zone- develops between the fault core and the damage zone, and significantly affects groundwater flow (Mozley and Goodwin, 1995). For instance, the Sand Hill fault is a steeply-dipping, large-displacements normal fault that cuts poorly-lithified Tertiary sediments of the Albuquerque basin, New Mexico, and measurements of permeability of the distinct fault-zone architectural elements show that the structures of these elements are different from brittle faults formed in lithified sedimentary and crystalline rocks (Rawling et al., 2001). The resulting bulk hydrologic properties significantly impede horizontal subsurface fluid flow at a regional scale and do not greatly enhance vertical flow, which is different than the previously described model of fault zones in consolidated rocks (Caine et al., 1996).

The characterization of faults components and their permeability is difficult since 1) it is often hard to determine the morphological position (fault core, damage zone, or protolith) from which the samples were collected (Evans, 1990) and 2) because fault components are highly heterogeneous and anisotropic, and contain complex spatially varying patterns of both low and high permeability structures (Faulkner et al., 2010). A small number of high permeability pathways may control fluid flow, but the fracture aperture away from wells and the connectivity of these pathways is typically unknown (Evans, 1990; Long and

Billaux, 1987). For instance studies in mine tunnels using discrete fractures models (Long and Billaux, 1987) showed that only about 0.1% of the fractures essentially control permeability and that even if fracture orientation and aperture are known, we cannot predict a priori which fractures are conductive. Hence, fault zone permeability is governed both by the permeability of individual fault rocks and fractures, and critically by their geometric 3-D architecture (Lunn et al., 2008a). Then, the hydrologic behavior of fault zones at regional scales is hard to predict as it is not a simple function of fault zones local behavior. Additionally, the regional tectonic stress is another important factor controlling fault permeability. Critically stressed fault zones have indeed a much higher permeability than weak faults that are not oriented for failure in the current stress field (Barton et al., 1995), and there is a strong correlation between critically stressed faults and hydraulic conductivity in highly fractured crystalline rock.

An integrated approach that includes field geology, laboratory measurements, geophysical measurements, modeling (analytical and numerical) and direct observation through drilling (Faulkner et al., 2010) is needed to fully understand fluid flow across faults. Then fault architectural data along with data on large-scale parameters such as lithology, stress history, or length of the fault from a large number of field studies can be used as multivariate statistics and improve the estimate of fault permeability (Lunn et al., 2008b).

b. Study of fault architecture and permeability

Fluid flow around fault zones is studied by both structural geologists and hydrogeologists (Bense et al., submitted) and their contrasting approaches are discussed.

i. Structural geologists approach

Investigating outcrops in diverse settings, structural geologists characterize fault architecture and its related permeability and then design models that describe fault zone structure.

The 2-D or 3-D architecture of the fault zone can be defined through outcrop mapping, where the fault is well exposed. For instance, Jourde et al (2002) characterized stripe-slip faults in porous sandstone in the Valley of Fire State Park, Nevada by mapping outcrops. Subsurface fault zone structure can be characterized using seismic data although the spatial resolution may be limited (Koledoyem et al., 2003). Permeability of fault rocks can be measured on site using a mini-permeameter but only small sample volumes are possible. This method can lead to mapping of permeability across fault zones in detail. Mini-permeametry has been used in the oil industry since the late 1960s and provides a rapid and nondestructive measurement of permeability with a great accuracy. Laboratory core tests on rock samples are also carried out to measure the permeability of fault elements. However laboratory tests only give small scale patterns of permeability and do not quantify a representative permeability map across a fault zone.

Having characterized both the fault structure and the permeability of the different elements present in the fault zone, structural geologists design subsequently a model that predicts fluid flow across the fault.

Also, the fault zone is affected by fluid flow, and when groundwater flows through a fracture, minerals can precipitate along the fracture resulting in an impermeable infilled fracture. Then, by characterizing fault rock mineralogy and geochemistry, or elemental composition of fault components, water-rock interactions can be assessed, and give an insight in the present permeability structure (Caine and Minor, 2009; Evans and Chester, 1995).

Furthermore, deformation processes and timing, as well as paleoflow orientation have been used to determine faults influence on fluid flow (Knipe, 1993; Mozley and Goodwin, 1995). Inferences can be made from cementation patterns as an indicator of paleo-fluid flow conditions around fault zones. For instance, Breesch et al (2009) used detailed petrographic and geochemical analyses of calcite filled fracture networks in Triassic and Cretaceous carbonate strata of Northern Oman to reconstruct a paleo-fluid flow history along reverse faults. Depending on paleo-fluid flow history, fault zones in carbonate rocks have been reported with a very wide range of hydrogeological behaviour, from significant barriers where secondary cementation or smearing of low permeability material occurs, to effective conduits where dissolution along fault and fracture planes dominates.

Therefore, structural geologists characterize fault structure, measure detailed permeability of elements from the fault zones, and build numerical models often using discrete fracture network models. However they do not provide direct hydrogeological evidence of hydraulic behavior to test and refine their outcrop-based models.

ii. Hydrogeologists approach

Conversely, hydrogeologists collect detailed hydrogeological evidence from wells and springs and associate them with geochemical and temperature surveys to trace groundwater flow paths around faults zones (Bredehoeft, 1997), but do not characterize fault zone architecture.

Hydrogeologic methods are also used to determine the permeability of fault zones. For instance, packer tests are another way of determining the *in-situ* permeability of fault components or fractures. Packer tests measure the pressure response in an isolated section of well, and can then give the vertical profile for permeability. Also, large scale permeability or transmissivity of aquifers and fault zones within an aquifer can be achieved with pumping tests that also measure the pressure response in the well.

The first parameter that can be measured from wells is the water level, which leads to hydraulic head gradients that are evidence for permeability discontinuities. Anomalously high hydraulic gradients across fault zones can be interpreted as a low fault permeability so that the fault acts as a partial barrier to groundwater flow (Haneberg, 1995). For instance, Medeiros et al. (2010) collected hydraulic head data around a fault zone dominated by cataclastic deformation bands in a sandstone aquifer. Although permeability measured in the deformation bands was reduced by almost five orders of magnitude as compared to the host rock, the hydraulic head does not show a significant discontinuity between the two sides of the fault zone suggesting that the fault does not act as a barrier. On the other hand, Mayer et al. (2007a) reports water table drops of 80 m across the Mission Creek fault, California, although the fault cuts through alluvium dominated by gravel in which clay-smearing along the fault plane is unlikely to occur. Also, contrasts in vegetation on either side of a fault can indicate differences in water table levels and then can be used as a proxy for hydraulic head discontinuity (Mayer et al., 2007b). However simple analyses of hydraulic head gradients only give preliminary results about the directions and rate of groundwater flow and therefore the potential change in permeability induced by the fault, but they are insufficient to delineate flow paths in fault zone.

Natural tracers for groundwater such as salinity, temperature and other geochemical parameters, or data on groundwater age provide additional constraints on fluid flow paths around fault zones and can constrain flow paths across fault zones when used in conjunction with hydraulic head observations. When the groundwater flow is significant enough, it perturbs the background geothermal gradient, and the delineation of the fluid flow paths is made possible by mapping groundwater temperature. For example, in the Lower Rhine Embayment in Germany, thermal anomalies occurring in the aquifers flanking the Rurrand fault can only be explained by significant along-fault up- and downwelling of groundwater and subsequent lateral migration into the aquifer (Bense et al., 2008). Also, springs often occur along faults and water discharges with elevated temperatures. The well-documented distribution and variation of temperature of springs along fault zones in the Northwestern Great Basin, USA is clear evidence that faults in crystalline and volcanic rock can be conduits, and the discharge of water near the boiling point in springs is indicative of rapid, upward advective transport along preferential flow pathways of enhanced permeability (Anderson and Fairley, 2008; Fairley and Hinds, 2004). Thermal springs that are more than 15˚C warmer than the surrounding air are indicative of high discharge through a fault. For example, the Bath hot spring discharges from a fault zone conduit in carbonate rocks in southwestern England (Andrews et al., 1982; Billi et al., 2007). In other cases where the springs occur at the surface coincident with a fault, the springs are indicative of the fault acting as a barrier (Celico et al., 2006; Giurgea et al., 2004). Heat flow data along faults can also give evidence for the strength of the fault (Saffer et al., 2003).

The application of saline tracers to a fractured thrust fault aquifer in Virginia, USA suggests that faults in crystalline rock can be combined conduits and barriers. A first tracer applied above a vertically oriented thrust fault zone traveled 160 m downgradient along the thrust fault subcrop within 24 days. A second tracer applied above a saprolite aquifer demonstrated high conductivity preferential flow pathways in the regolith near the bedrock surface, while a small proportion of the second tracers are found in the underlying fault zone (Rugh and Burbey, 2008). This confirms previous results from Seaton and Burbey (2005) who used surface and wells geophysics, such as water-level contours and geologic cross section, and aquifer tests along with chlorofluorocarbon and geochemical data and demonstrated that the shallow high permeability saprolite aquifer is separated from the deeper fault zone aquifer by a low-fracture permeability bedrock confining unit. Recharge and discharge occur by slow leakage through the confining unit or through localized breach zones that occur where quartz accumulated in high concentrations during metamorphism and later became extensively fractured during episodes of deformation, which explains why a part of the tracer was found in the deep aquifer. Flint et al (2001) used bomb pulse isotopes (e.g. ^{36}Cl) which were highly elevated in the atmosphere during nuclear testing in the Pacific Ocean in the early 1960s to assess groundwater ages. The presence of these isotopes in groundwater in fault zones indicates that groundwater is less than 40 years old, suggesting a deep, rapid and preferential infiltration along the faults.

In order to better constrain fault zone permeability an integrated approach that includes field geology, numerical modeling as well as field hydrogeology is necessary (Faulkner et al., 2010). Integrative numerical modeling of fluid flow patterns across a fault zone can be designed for both discrete feature models, and continuum models using effective fault zone properties, and hydrogeological data. These integrate wells and outcrop data and enable the testing of conceptual models and parameter estimations.

c. Study of interactions between surface water and groundwater

The field of 'groundwater-surface water interactions' which connects hydrogeology and hydrology has recently been growing rapidly (Hayashi and

Rosenberry, 2002; Kalbus et al., 2006; Sophocleous, 2007). Groundwater flow into any water body, called groundwater discharge, can be characterized through a number of different methods using various environmental tracers, such as water temperature, solid particles, ionized substances, stable isotopes, radioactive tracers, chlorofluorocarbons, or artificial tracers such as dyes. The artificial tracers are becoming less used since naturally occurring tracers have been found to be powerful enough, and non-invasive methods are preferred. Heat can be used to delineate flows in the hyporheic zone, estimate submarine groundwater discharge and depth to the salt water interface, and in parameter estimation with coupled groundwater and heat flow models (Anderson, 2005).

Lately, naturally occurring radon (^{222}Rn) has been widely used to quantify groundwater discharge to rivers (Cook et al., 2003; Cook et al., 2006; Genereux et al., 1993), wetlands (Cook et al., 2008), lakes (Dimova and Burnett, 2011; Gleeson, 2009; Kluge et al., 2007), or oceans (Cable et al 1996). Radon-222 (^{222}Rn) is a radioactive noble gas produced by natural decay of radium-226 (^{226}Ra), which is part of the natural decay chain of uranium-238 (^{238}U). Its short half-life of 3.82 days makes it a useful tracer in environmental investigations. Radon occurs naturally in rocks and soils in various concentrations which is directly determined by the local amount of parent radionuclide present, and is generally small (less than a part per million or less) (Cecil and Green, 1999). It is found in large concentrations in granitic rocks that contain elevated concentrations of uranium (ten or more parts per million) (Hall et al., 1987). Its occurrence varies widely, even over relatively short distances and within the same environment, as its parent radionuclides must be present throughout the rock in isolated groups, or in significant but varying amounts along fracture walls and near the surface of the rock. Most of radon that is produced decays inside rocks and only a small amount can escape from the rock, through direct or indirect recoil (Cecil and Green, 1999). Once it has escaped from the rock, it can freely move into the pore spaces, into fractures, or out of the rock, and migrate with groundwater, to surface water or to the air, where it decays quickly. Due to the large difference in activities between groundwater and surface water, its non-reactivity, and its rapid decay, radon is a powerful, efficient and accurate groundwater tracer (Dimova and Burnett, 2011).

Steady-state advective models based on radon mass balance lead to quantification of water discharge, while the patterns of groundwater discharge can be characterized by the distribution of temperature, or various geochemical tracers. For instance, Gleeson (2009) estimated the rates of groundwater discharge and surface water inflow to lakes and wetlands in a large watershed in the Canadian Shield using radon and chloride mass balance that includes groundwater discharge, surface water outflow, precipitation, evaporation, gas exchange and radioactive decay for radon. Then, plotting the radon activity, as well as the temperature and specific conductance along a 25-km long transect showed that the groundwater discharge is distributed throughout the watershed and that it is not localized around lineaments or high-density zones of exposed brittle fractures. Kluge et al (2007) quantified the groundwater discharge rate to a small lake in the Rhine Valley using a model considering radon inflow through groundwater discharge, and diffusive flux from sediments and radon outflow through groundwater recharge, gas exchange, and radioactive decay. Mapping the vertical profile of radon activity in the lake, the location of groundwater discharge was found to be located mainly to the upper part of the lake. Cook et al. (2008) also estimated the mean groundwater inflow to a shallow wetland in Southern Australia from a mass balance of radon. The radon budget takes into account the contribution from groundwater inflow, the diffusive flux from wetland bottom sediments, the loss due to gas exchange, the loss due to radioactive decay, and the loss due to groundwater or surface water outflow. Because of the small lake's depth, the percentage loss due to gas exchange was high, and inferred from the loss rate of SF_6 injected into an isolated area (Cook et al., 2008). For deeper lakes, the sensitivity to gas exchange rate decreases and the main mechanism for radon loss is decay. Also, for lakes with a significant groundwater inflow rate, the diffusive flux from sediments becomes a minor radon source and can be neglected. Finally a major difficulty arising when studying shallow wetlands with depths of less than 1 meter is that mixing does not perfectly occur. Then, the vertical and horizontal profiles of concentrations need to be investigated to estimate the average concentrations in the lake.

Although groundwater discharge has been studied qualitatively in fractured bedrock aquifers (Oxtobee and Novakowski, 2002; Praamsma et al., 2009), methods developed in the field of groundwater-surface water interactions using radon have not been applied to fluid flow around faults.

III. **Field areas**

Three study areas are shown in Figure 3. Our present study was carried out in the first two areas, located in the Appalachian Mountains in southern Québec, Canada in Sept-Nov, 2011. The southern area (Figure 3b) is located around Magog, about 100 km east of Montreal, in the Eastern Townships. The northern site (Figure 3c) is located around Thetford-Mines, about 100 km south of Québec City, in the region of Chaudière-Appalaches. The third area shown in Figure 3a, corresponds to the study carried out by Gleeson et al. (2009) in the Canadian Shield, that we use as a comparison for our results. It is located in rural eastern Ontario, Canada, in the ~900 km^2 Tay River watershed. The hydrology, climatology and geology of this area are described by Gleeson et al. (2009).

The lakes we sampled are mainly minor lakes with areas ranging from 0.05 to 4 km^2. We sampled 34 lakes in the southern area, within a radius of 30 km, and 20 lakes in the northern area also within a radius of 30 km. Few streams typically enter the lakes, some of the lakes having no discernible or mapped inlet. Some lakes are independent without nearby lakes in their watershed whereas other lakes are part of small interconnected lake systems. The water temperature of our samples ranged from 20°C at the beginning of the fall to 5°C at the end of the sampling, in early November 2012.

Both regions have undulating valley and ridge topography with gentle relief with up to 800 m of elevation. There are very few agricultural activities, and the land is mainly covered with deciduous forest dominated by sugar maples, yellow birches, beeches and red oaks.

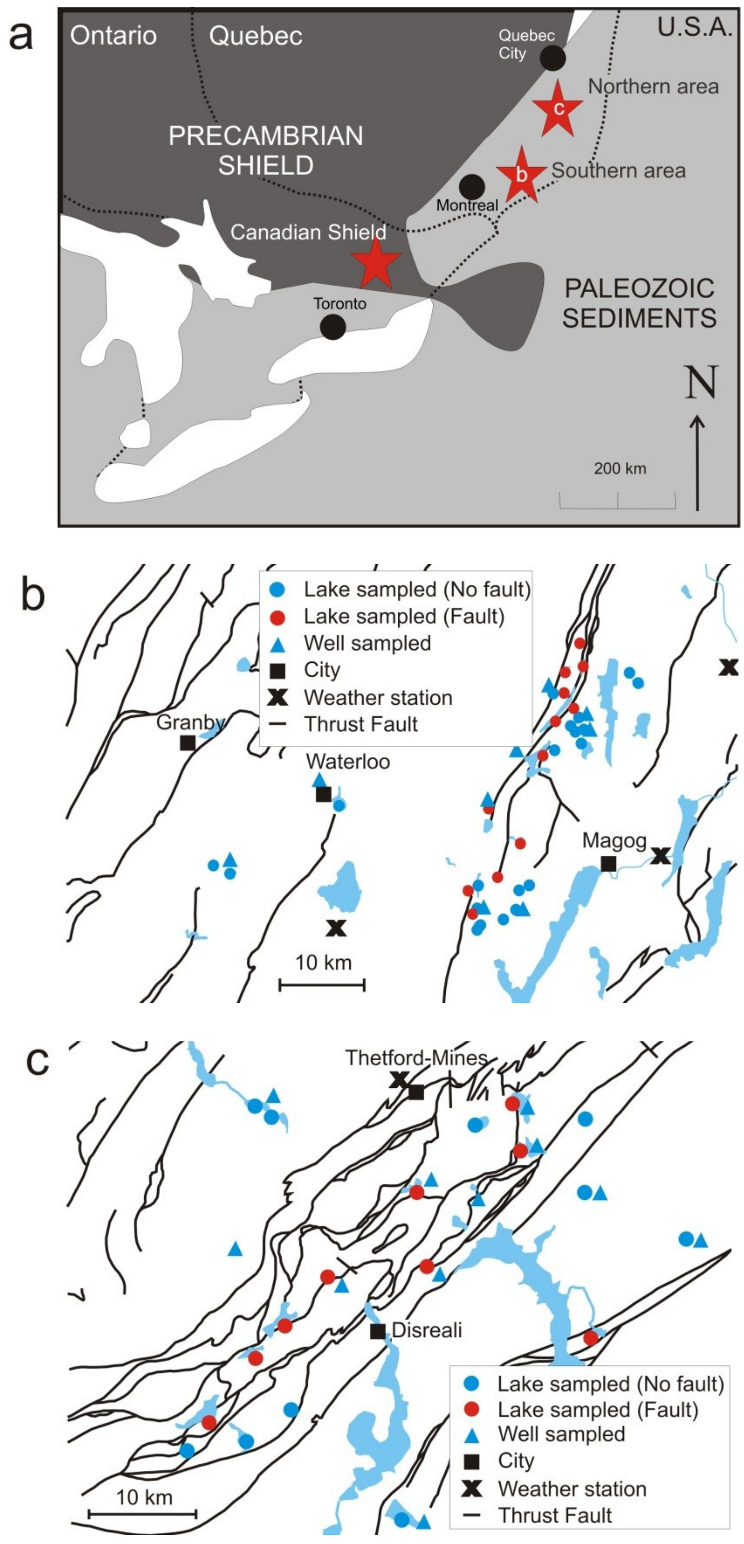

Figure 3: (a) Study area. The sampling area was divided in two zones: the (b) southern area, with 34 lakes sampled, and the (c) northern area, with 20 lakes sampled. The third area shown in (a) is the region of Gleeson study (2009) in the Canadian Shield.

The whole area has a humid continental climate, with daily temperatures ranging from -16°C to 25°C. The average temperature during our sampling is ~10°C. The annual precipitation ranges between 900 and 1,000 mm, and the annual snowfall is between 200 and 400 cm. The average precipitation is ~100 mm, 90 mm and 70 mm respectively in September, October and November.

The thrust faults are all part of the Appalachian orogenic front deformed during the Ordovician Taconian orgogeny (Séjourné and Malo, 2007). The thrust fault zones cross-cut and deform Paleozoic sediments (slates, feldspathic sandstone and conglomerates) as well as an ophiolitic sequence comprised of serpentinite, pyroxenite and volcanics (St-Julien and Slivitzsky, 1985). The thrust slices are locally intruded by a Cretaceous gabbro.

IV. Methods

a. Analytical model

i. Theory

Gleeson et al. (2009) developed a steady-state advective model using radon (^{222}Rn) and chloride budgets for quantifying groundwater discharge rates. Radon is a radioactive gas produced within the uranium decay series, with a short half-life (3.8 days). It has a high activity in groundwater whereas activities in surface water are low due to radioactive decay and gas exchange and negligible in precipitation. Chloride also has a higher concentration in groundwater than in surface water, and unlike radon, it is a dissolved constituent that does not evaporate. The mass balances of these complementary tracers are combined to estimate the groundwater discharge rate.

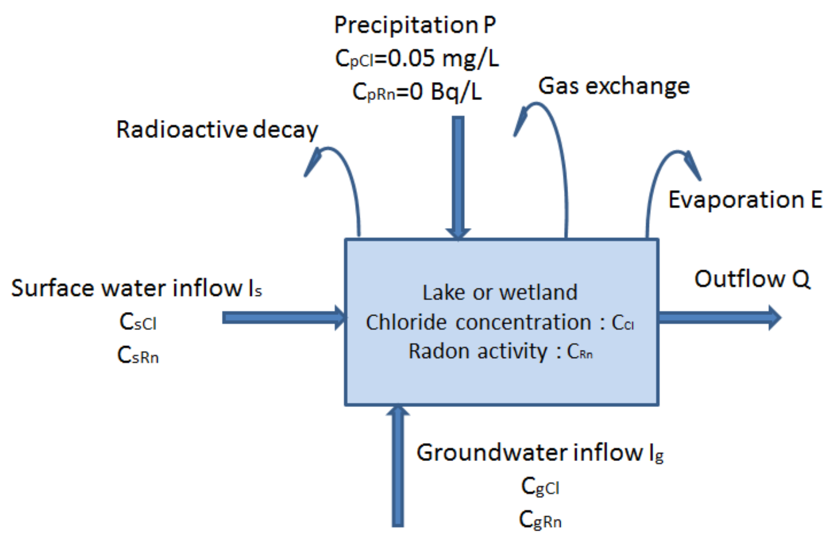

Figure 4: Schematic of the steady-state model. Variables names are explained in the table below.

Table 1: Nomenclature

A	*Lake area (m^2)*
$\mathbf{C_{Cl}}$	*Mean chloride concentration in lake (mg/L)*
$\mathbf{C_{Rn}}$	*Mean radon activity in lake (Bq/L)*
$\mathbf{C_{gCl}}$	*Mean chloride concentration in groundwater (mg/L)*
$\mathbf{C_{gRn}}$	*Mean radon activity in groundwater inflow (Bq/L)*
$\mathbf{C_{pCl}}$	*Mean chloride concentration in precipitation (mg/L)*
$\mathbf{C_{sCl}}$	*Mean chloride concentration in surface inflow (mg/L)*
$\mathbf{C_{sRn}}$	*Mean radon activity in surface inflow (Bq/L)*
d	*Mean lake depth (m)*
E	*Evaporation rate (m/day)*
$\mathbf{I_g}$	*Groundwater inflow (m^3/day)*
$\mathbf{I_s}$	*Surface water inflow (m^3/day)*
k	*Gas exchange velocity (m/day)*
P	*Precipitation rate (m/day)*
Q	*Surface and groundwater outflow (m^3/day)*
V	*Lake volume (m^3)*
$\boldsymbol{\lambda}$	*Radioactive decay coefficient (day^{-1})*

Using this steady-state advective model we estimated the groundwater discharge rate to each of the 54 sampled lakes. By subsequently comparing groundwater inflow into the 21 lakes located on a fault, and the 33 lakes located away from any fault, we can assess the impact of the fault zones on the hydraulic properties of the rock or soil beneath the lake.

The steady-state water budget is summarized in Figure 4. It is expressed as:

$$\frac{\partial V}{\partial t} = I_s + I_g + P \cdot A - E \cdot A - Q = 0 \qquad (1)$$

where the combined groundwater and surface water outflow Q can then be expressed as a function of I_s, the surface water inflow rate (m^3/day), I_g the groundwater inflow rate (m^3/day), P the precipitation rate (m/day), A the surface water area (m^2), and E the evaporation rate (m/day).

For the chloride, the inflow from surface water, groundwater, and precipitation are balanced with the outflow Q, leading to the following equation:

$$C_{Cl} \cdot Q = I_S \cdot C_{s,Cl} + I_g \cdot C_{g,Cl} + P \cdot A \cdot C_{p,Cl} \qquad (2)$$

Where C_{Cl} is the chloride concentration in the lake, $C_{s,Cl}$ is the chloride concentration in the incoming surface water, $C_{g,Cl}$ is the chloride concentration in the groundwater, and $C_{p,Cl}$ is the chloride concentration in precipitation.

For the radon, which does not occur in precipitation, the inflow from surface and groundwater is balanced with the outflow, the radioactive decay, and the gas exchange as describes the equation:

$$C_{Rn} \cdot (Q + k \cdot A - \lambda \cdot V) = I_s \cdot C_{s,Rn} + I_g \cdot C_{g,Rn} \qquad (3)$$

Where λ is the radioactive decay constant (day^{-1}), V the volume of the lake (m^3), k the gas exchange velocity (m/day), C_{Rn} is the radon activity in the lake, $C_{s,Rn}$ is the radon activity in the incoming surface water, and $C_{g,Rn}$ is the radon activity in the groundwater. We assume indeed that both the diffusive radon flux from the lake sediments and the radium activities in the lake are negligible.

Equations 1, 2 and 3 were simultaneously solved for each lake to determine the three unknown factors I_g, I_s and Q. For the lakes with no major inlets -19 lakes are concerned-, the discharge rate is calculated taking I_s=0.

ii. Field sampling and laboratory analysis

Field work was conducted during low flow conditions in the late summer and early fall 2011 in the Eastern townships and Chaudière-Appalaches, Quebec. Lakes were sampled from either private docks, boats or directly from the shore for both chloride (C_{Cl}) and radon (C_{Rn}) analysis (Figure 5c). Water was sampled about 10 to 20 cm under the surface in order to minimize air contamination, and to be within the epilimnion whose radon activity corresponds approximately to the lake average (Kluge et al., 2007).

All major inlets were also sampled, to determine inflowing chloride concentrations ($C_{S,Cl}$) and radon activities ($C_{S,Rn}$). Samples were taken, usually from the river bank or from a boat, as close to the lakes as possible and about 10 to 20 cm under the surface to minimize the effect of air exchange. The low-flow conditions ensured the measurement of representative concentrations in the creeks. When more than one stream was discharging to the lake, the inflowing activities for both chloride and radon was estimated by a stream flow-weighted mean. Stream flow was measured with a propeller with a precision of 0.1 m/s, estimating the flow of 5 to 10 points on a transect of the stream, where the water was sampled (Figure 5a).

Groundwater samples were collected from 20 private wells across our study area along with lakes and creeks sampling (Figure 3). The depths of wells range from 20 to 100 meters below ground surface. The water was collected mainly from outside taps, ensuring that the water was unfiltered (Figure 5b). Since the concentration of radon in groundwater varies widely even over short distances, we were not able to accurately estimate the radon activity in groundwater that discharges to each lake. Instead we use the mean value for $C_{g,Rn}$ for all the lakes, and assess the uncertainty due to the natural variability of radon activities, as described below. Similarly we use the mean value for chloride concentration in groundwater $C_{g,Cl}$, and used a statistical approach to assess the uncertainty of our model due to the variability of chloride concentration in groundwater.

a.

b.

c.

Figure 5: (a) Flow measurements with a propeller. (b) Well sampling, with a syringe to minimize air-contact and loss of radon through gas exchange. (c) Lake sampling, from a private dock.

Lake area (A) was derived from Canmap using ArcGIS DMTI (2010). Lake depths were derived from a report by Prairie and Soucisse (1999) or from field measurements and estimations. Lake volume (V) was estimated from the area and depth of each lake. The precipitation rate (P) was assessed, from the daily values at four meteorological stations in the Eastern Townships and Chaudière-Appalaches: Magog (45°16'N;72°07'E), Brome (45°11'N;72°34'E), Bromptonville (45°29'N;71°57'E), and Thetford-Mines (46°06'N;71°21'E). Because of the three days half-life of radon, the time period considered for the model is about a week. Then, an average over the week preceding the sampling was computed for each lake, using the station in Thetford-Mines for the lakes within the northern region, and an average on the three other stations for the lakes in the southern region. Chloride concentration in precipitation ($C_{P,Cl}$) was extracted from the *Canadian National Atmospheric Chemistry database*, at the station in Frehligsburg (45°03'N;72°51'E), about 50 km south-west of the southern study area. Radon activity in precipitation is assumed to be negligible.
Our analysis included data on the watershed areas and topography which we analyzed in ArcGIS using the digital elevation model derived from Geobase Canada (2012). Topographic gradients were estimated manually whereas watersheds area were determined using the watershed function from the spatial analyst tool.

The radioactive decay constant for radon is $\lambda = 0.18\ d^{-1}$. Cook et al. (2008) estimated the gas exchange velocity for radon k from measurements of the gas transfer rate between a wetland and the atmosphere of an injected tracer, SF_6, carried out in Australia. The measurements lead to a gas transfer velocity of *k=0.16* m/day, which is the value we adopted. The steady-state model is not very sensitive to the gas transfer velocity since the lakes are relatively deep (Cook et al., 2008). Moreover the emphasis of our study is to assess the difference between lakes and so an error in the gas exchange rate will shift all our results and will not change our conclusion. Radioactivity of radon was measured using the liquid scintillation counter *Hidex 300 SL* with a detection limit of 0.02 Bq/L. Chloride concentrations were measured using ion chromatography, with a detection limit of 0.1 mg/L.

iii. Sensitivity analysis

The sensitivity of the model to all its input variables was tested using two methods. First, we observed the variations of the discharge rates as a function of each parameter for a 'typical' lake, whose parameters are taken as the average value of the values of the 54 lakes. Second, we computed the groundwater discharge rate for each lake, varying each parameter individually by ±20% and by ±50%.

Then, the robustness of the results given the uncertainty in the measured parameter values was investigated using a Monte Carlo approach. First, we estimated the error in the estimation of the discharge rate caused by the uncertainty in the radon activity in groundwater. Radon activity in groundwater is indeed difficult to estimate accurately because of its high heterogeneity, even at the lake scale. We therefore ran the steady-state model for each lake 5000 times, varying the value of radon activity in groundwater, whereas all other parameters remained constant. The value of radon activity in groundwater is computed for each simulation as a random variable that follows a lognormal distribution with the mean and the standard deviation of the 20 groundwater samples. The distribution of the resulting discharge rates was then compared to the previously estimated value.

We assessed subsequently the effect of the cumulative uncertainty of all the model parameters (lake area, lake depth, radon activity in lake, inflow and groundwater, chloride concentration in lake, inflow, groundwater and precipitation, and precipitation and evaporation rates) on the calculated discharge rate to each lake. We carried out a global Monte Carlo simulation, calculating the discharge rate for 5,000 simulations for each lake, while varying all variables simultaneously. Each variable was considered as a random variable following a normal distribution with a mean equal to the previously estimated value, and a standard deviation equal to 20% of the mean. Again, the distribution of the groundwater discharge rates was compared to the previously estimated values.

iv. Statistical analysis

The comparison between the results of groundwater discharge rates to lakes overlying faults and other lakes was conducted using two two-sample statistics tests: the Welch's t-test, and the Kolmogorov-Smirnoff's test (Lilliefors, 1967; Marsaglia et al., 2003; Massey, 1951; Miller, 1956). The Welch's method tests the null hypothesis stipulating that the means of both data sets are equal, whereas the

Kolmogorov-Smirnoff's method tests the null hypothesis stipulating that both data sets are from the same continuous distributions.

For the Welch's t-test the t-statistic is:

$$t = \frac{\overline{X_f} - \overline{X_o}}{s_{\overline{X_f} - \overline{X_o}}}$$

Where X_f and X_o are the means of the estimated discharge rates for respectively the lakes overlying a fault and the others, and:

$$s_{\overline{X_f} - \overline{X_o}} = \sqrt{\frac{s_f^2}{n_f} + \frac{s_o^2}{n_o}}$$

s_f^2 and s_o^2 are the unbiased estimations of the variance of the discharge rates for the lakes with a fault and without a fault respectively. n_f and n_o represent the number of lakes with and without faults, respectively. Then, the p-value is computed from the test statistic distribution, at the confidence level α, taken equal to 5%, and for the effective degree of freedom ν that is approximated using the Welch-Satterthwaite equation:

$$\nu = \frac{\left({s_f^2}/{n_f} + {s_o^2}/{n_o} \right)^2}{\left(\frac{s_f^2}{n_f} \right)^2 / (n_f - 1) + \left(\frac{s_o^2}{n_o} \right)^2 / (n_o - 1)}$$

The null hypothesis that stipulates that the means of the groundwater discharge rates to the lakes underlain by a fault and to the other lakes are equal is rejected if the p-value is smaller than the confidence level α.

For the Kolmogorov-Smirnoff's test, the ks-statistic D_{n_f, n_o} is:

$$D_{n_f,n_o} = \max_x \left| F_{f,n_f}(x) - F_{o,n_o}(x) \right|$$

Where F_{f,n_f} and F_{o,n_o} are the empirical distribution functions of respective samples for the lakes with an underlying fault and the other lakes.

Then, the null-hypothesis that stipulates that the distributions of the discharge rates to lakes with an underlying fault and to the other lakes are the same is rejected if:

$$\sqrt{\frac{n_f n_o}{n_f + n_o}} \cdot D_{n_f,n_o} > K_\alpha$$

Where the critical value K_α for the confidence level α can be found in tables (Miller, 1956).

The same tests were performed to compare the data from our study in the Appalachian orogen with the data from the study carried out by Gleeson (2009) in the Canadian Shield, to assess whether the impact of faults on the groundwater discharge could be more important than the type of the surrounding bedrock. We also used both statistic tests to study the results of both Monte Carlo simulations. We computed Welch's and Kolmogorov-Smirnoff tests for each of the 5,000 simulations, and we estimated the frequency of rejecting the null-hypothesis suggesting that groundwater discharge rates are the same in presence of a fault zones. Both statistic tests were also run to compare the simulated data with the data from the Canadian Shield.

b. Numerical model

In order to better understand the differences in groundwater discharge rates that we estimated for the 54 lakes we sampled, we simulated the effect of lake width, the topographic gradient, watershed area, fault zone permeability and fault width on the groundwater discharge to lakes underlain by fault zones or not, using a two-dimensional, steady-state finite-element numerical model. The USGS code SUTRA was chosen because it is a well-tested finite-element code for groundwater flow (Voss, 2002). The 2-D model is represented in Figure 6a. It includes two lakes, Lake 1 and Lake 2, located along a regional topography gradient. As an illustration, Figure 6b shows a similar geometry including two lakes we sampled along a regional topography gradient in the Appalachian orogen.

We are modeling an idealized system with reasonable parameter values for topography, geometry, and permeability. The model computes the groundwater discharge rate to Lake 1. Groundwater flow is driven by a regional topographic gradient from left to right. The geometry of the recharge area located upgradient of Lake 1 was varied in our modeling: the topographic gradient ranged from 10 to 50%, and the length of the recharge zone was varied from 0.5 to 2 km. The width of Lake 1 was varied from 0.1 to 1 km, and both lakes have a constant head boundary that is determined by their average lake level. The remaining top boundary to the ground surface was assigned a constant recharge rate of 100 mm/month. The aquifer is saturated and 300 meters deep. The lateral and bottom boundaries were no-flow boundaries. The underlying bedrock was assigned a 10:1

anisotropy ratio of hydraulic conductivity, with a horizontal conductivity of 10^{-7} m/s and a vertical conductivity of 10^{-8} m/s. The fault underlying Lake 1 is modeled by a vertical zone with an internally homogeneous and anisotropic hydraulic conductivity that differed from the surrounding rock.

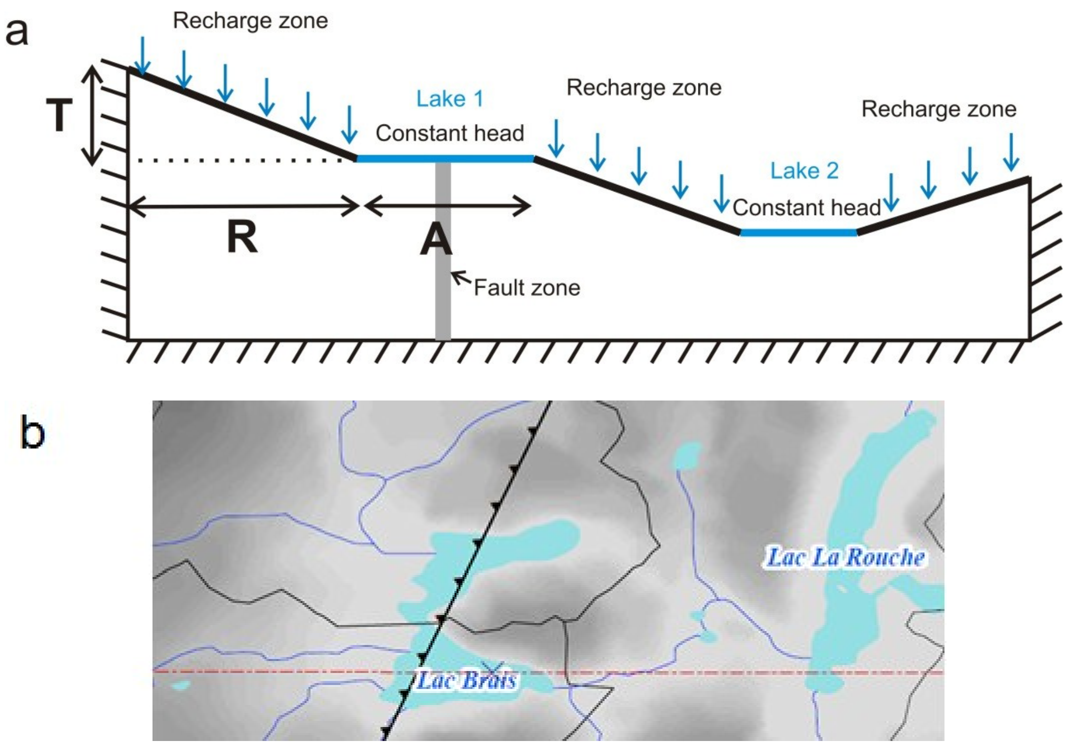

Figure 6: (a) Schematic of the numerical 2-D model. The topographic gradient (T), the recharge area (R), and the lake area (A) are varied. The groundwater discharge to Lake 1, which is overlying the fault zone is calculated. Fault zone width and permeability structure are also varied. As an example (b) shows a map including two lakes sampled: Lac Brais that corresponds to Lake 1 of the model and Lac La Rouche that corresponds to Lake 2. The fault is schematized as a line with triangles, and the red line shows the cross-section along which the 2-D model was designed.

Two fault zone widths were tested: a thin fault zone (10 m), and a thick fault zone (100 m). We simulated a vertical fault zone although this might not be the case for the fault zones we studied, because a vertical fault zone has potentially the most significant effect on the groundwater flow in our 2-D model. In that way, we could ensure that the model did not underestimate the impact of the fault zones on the regional permeability. Moreover, the fault zone permeability was modeled using a composite permeability structure combining the fault core and the damage zone. The permeability of the fault zone is controlled by the distribution of fault zone components and a small proportion of the fractures which are both uncertain for the fault zones we examined. Therefore we consider the hydraulic conductivity in the fault zone as a bulk property rather than considering contributions from individual fault zone components or fractures which is consistent with the generalized goals of the modeling and the lack of precise, local-scale data.

Three fault zone permeability structures were investigated. First a fault zone acting as a barrier to flow, with both vertical and lateral hydraulic conductivity reduced. Then we tested a scenario with a fault zone acting as a combined vertical conduit and lateral barrier and finally the structure where the fault zone acts as a distributed conduit with both vertical and lateral hydraulic conductivity enhanced. For the three configurations, the fault zone was modeled as a composite equivalent porous-medium with homogeneous and anisotropic hydraulic conductivity that is the composite of the fault core and damage zone. Depending on the chosen permeability structure, the hydraulic conductivity of fault zones was increased or decreased by two orders of magnitude relative to the surrounding bedrock, to emphasize the effect of the fault zone on groundwater flow (Table 2). The purpose of this modeling part is to observe the qualitative effects rather than quantify the actual flow rates so that we tried out different permeability structures rather than attempting to calibrate our results to the discharge rates calculated above. The fourth permeability structure described in the literature (Caine et al., 1996) - fault acting as a localized conduit to flow - was not modeled here, as it needs a discrete fracture network model rather than an equivalent porous medium. However the conduit structure can be understood as a small-width distributed conduit, and the results could be interpolated for a conduit structure.

Table 2: Values of 2-D hydraulic conductivities in the fault zone for different permeability structures. In all cases, the hydraulic conductivity of the surrounding rock is $K_x = 10^{-7}$ m/s and $K_z = 10^{-8}$ m/s

	K_x - Horizontal hydraulic conductivity (m/s)	K_z - Vertical hydraulic conductivity (m/s)
Barrier	10^{-9}	10^{-10}
Vertical conduit	10^{-9}	10^{-6}
Distributed conduit	10^{-5}	10^{-6}

V. Results and discussion

a. Analytical model

i. Field and laboratory results

Radon and chloride activities of all the water bodies sampled are shown in Figure 7. Groundwater samples consistently have a higher radon activity than surface water samples. Indeed the mean radon activity in groundwater (54 Bq/L) is two orders of magnitude higher than in surface water (0.5 Bq/L for creeks and 0.3 Bq/L for lakes). This confirms the validity of radon as groundwater tracer. The distribution of radon activity in the lakes is relatively well distributed with 5 extreme outliers with radon activities of 5.2 Bq/L, 2.5Bq/L, 2.2 Bq/L, 0.9 Bq/L and 0.7 Bq/L (Figure 7b). These high values are evidence for high groundwater discharge. The remaining lakes have an average radon activity of 0.15 Bq/L. All the samples have higher radon activity than the radon detection limit of the liquid scintillation counter, equal to 0.01Bq/L. The mean radon content in lakes, with an average of 0.32 Bq/L is high in this area, as compared to the Canadian Shield where the average activity of radon in the lakes was about 0.009 Bq/L (Gleeson et al., 2009). This suggests that the groundwater discharge is high in this orogenic study area with sedimentary and volcanic bedrock, as compared to the crystalline bedrock in the Canadian Shield.

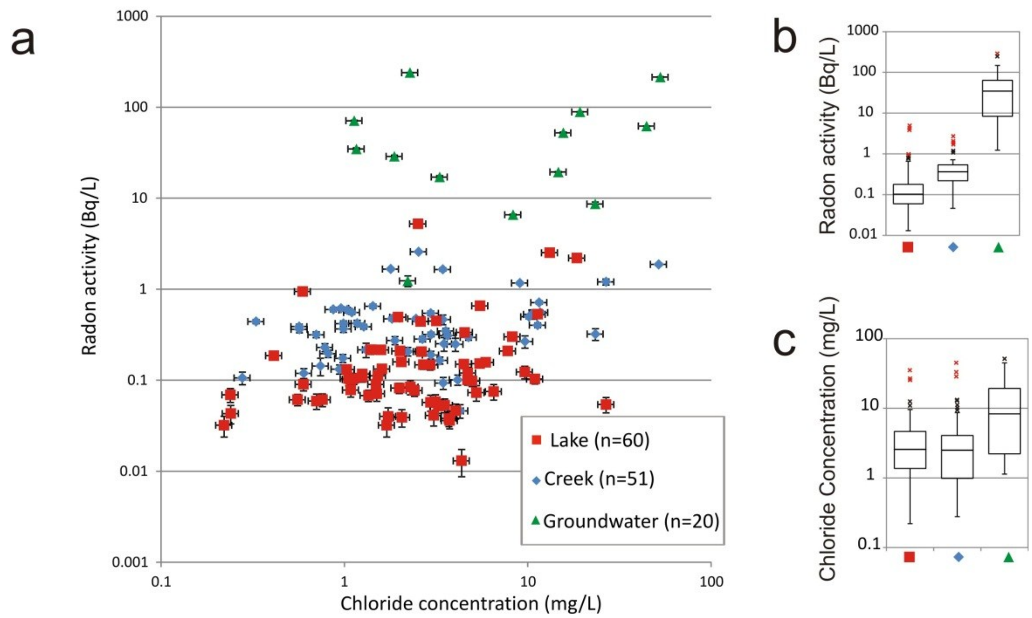

Figure 7: (a) Radon activity and chloride concentration for the three types of water bodies sampled: lakes, creeks and groundwater. The error bars are measurement errors and do not account for the potential uncertainty due to sampling location and time. (b) and (c) show the boxplot representing the distribution of respectively radon activities and chloride concentrations in the data. The boxes include 50% of the samples, from the first quartile (Q1) to the third quartile (Q3). The negative error bar indicates the minimum observed value, and the positive error corresponds to one and a half interquartile range. The outliers (black x) are defined as the values above the positive error bar and are described in the text. The extreme outliers (red x) are defined as the points exceeding the third quartile by more than three interquartile ranges.

Radon activity in groundwater is relatively heterogeneous, and the standard deviation (65 Bq/L) is higher than the mean (54 Bq/L) if all samples are included. Figure 8b shows the radon activity measured in the wells in the southern area (Magog and Bromont), in the northern area (Disraeli), as well as the values measured by Gleeson et al. (2009) in the Canadian Shield. The two wells sampled in the Bromont area show a much higher radon activity than the other wells, respectively 240 Bq/L and 214 Bq/L. The two regions correspond to a gabbro intrusion (see Figure 8c) with magmatic rocks which likely explains the high radon activity. Hence we assigned the three lakes (Waterloo, Bromont and Gale) in the Bromont region a different value for the radon activity in groundwater, equal to the average of both samples (227 Bq/L), and we excluded both values for the averaged estimation of radon activity in groundwater, which is then 34.5 ± 28.8 Bq/L. The standard deviation is high, as it represents more than 80% of the average value. The radon activity in groundwater is typically quite variable due to the variable production and transport of uranium (Folger et al., 1996). Therefore we consider our average value a reasonable estimation of the average groundwater that discharges to the lakes in the study area.

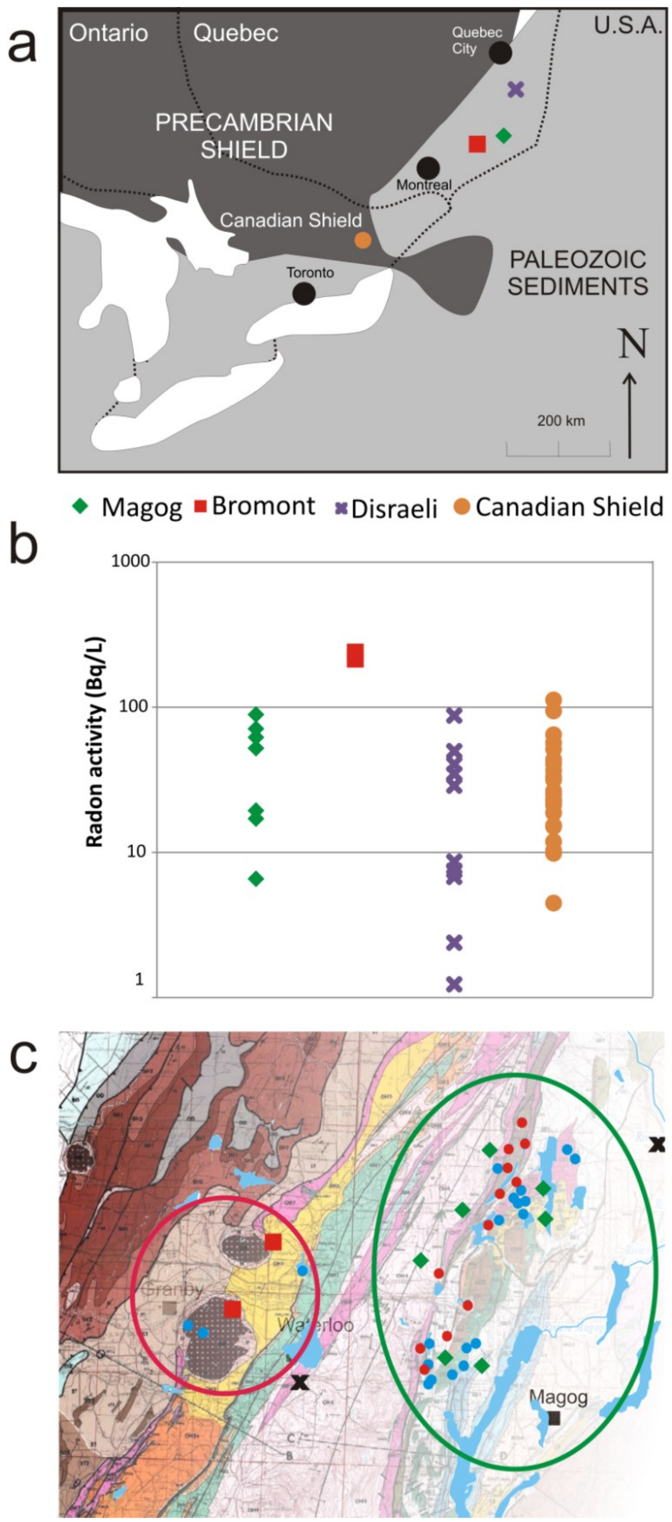

Figure 8: Radon activity in our groundwater samples for 4 groups of lakes. (a) Location of the 4 areas. (b) Radon activity for the samples from each group. Bromont shows higher radon activity than the three other areas. (c) Geology of the southern area (Bromont and Magog). The two samples in Bromont area are located on a gabbro intrusion, shown in brown (St-Julien and Slivitzsky, 1985).

Chloride concentrations in the samples are much more broadly distributed with overlapping typical concentrations for the different types of water bodies. The average chloride concentration in groundwater (13.8 mg/L, with a standard deviation of 18 mg/L) is higher than the surface water chloride, (5 and 4.1 mg/L with standard deviation of 8.5 and 4.8 mg/L, respectively for creeks for lakes) but the difference is not as significant as for radon. Also, lakes and creeks have comparable chloride, making it more difficult to differentiate these water bodies. Moreover, chloride as a groundwater tracer is less reliable than radon, as it can come from other sources and has a long residence time in surface water. However, those two considerations do not significantly affect the accuracy of our results, since the sensitivity of our model to chloride concentration is much lower than to radon activities, as detailed below.

ii. Steady state model

Using the steady-state model we estimated the groundwater discharge rate to each of the 54 lakes. The groundwater discharge rates are plotted in Figure 9 against three topographic and geometric parameters that control groundwater flow: the lake area, the watershed area, and the maximum topographic gradient, which is used as a proxy for the mean topographic gradient.

In Figure 9a, we plotted the calculated discharge rates for each lake against their areas, for both groups of lakes in the Appalachian orogen (the ones located on a fault and the ones located away from a fault), as well as for the lakes from the Canadian Shield that do not overlie a fault. As expected, the total discharge rate increases with lake area, which supports the overall validity of the analytical model. Also, the lakes from the Canadian Shield have on average smaller discharges than the lakes in the Appalachian orogen for a given lake area. The median discharge rate for lakes in the Appalachian orogen located on a fault (2.4 mm/day) is very similar to the median discharge rate for lakes that are not underlain by a fault zone (2.3 mm/day). The median discharge rate for lakes in the Canadian Shield is much lower (0.9 mm/day), suggesting that the groundwater discharge is more significant in the sedimentary and volcanic rocks of the Appalachians than in the crystalline bedrock. The discharge rates to lakes which are not underlain by a fault are more broadly distributed than those to lakes located on a fault zone.

Apart from that, their distributions are similar, and the two data sets cannot be differentiated on the boxplot (Figure 9a). The boxplot shows then that the discharge rates in the Canadian Shield are smaller than the discharge rates estimated in the Appalachians.

The groundwater discharge rate also depends on the recharge flux that occurred upstream, which can be approximated by the watershed area. Figure 9b represents the estimated discharge rates of the 54 lakes in the Appalachians plotted versus their watershed areas, estimated with ArcGIS. The groundwater discharge rate also increases with watershed area. The inset boxplot shows the distribution of the groundwater discharge rates normalized by the watershed area for both lakes overlying a fault zone and lakes that are not located on a fault zone. Again, the distributions of both data sets are very similar, except that the data is more broadly distributed for the lakes not underlain by a fault. The median ratio of the discharge rates to the watershed areas is 0.24 mm/day for the lakes overlying a fault and 0.14 mm/day for the other lakes. And 50% of the data are between 0.14 and 0.4 m/day for the lakes located on a fault, and between 0.05 and 0.4 m/day for the other lakes. Hence after normalizing the discharge rates to the associated watershed areas, there is still no discernible difference between the lakes located on a fault zone and the other lakes.

Although hydraulic gradients drive groundwater flow, there is no obvious correlation between maximum topographic gradient in a watershed and groundwater discharge rate (Figure 9c). Therefore, although we cannot exclude the fact that topography can control the groundwater discharge rate, topography does not explain the major differences between the calculated values of discharge rate. Furthermore, again there is no difference noticeable between the lakes located on fault and the lakes not underlain by a fault.

For all the further analysis, we use area-averaged flux (the groundwater discharge rate normalized by the lake area) for two reasons. First, area-averaged flux is effectively the Darcy flux which is proportional to the permeability, the parameter we are trying to characterize. Second, the discharge rates show the best correlation with the lakes areas with a relation quasi linear between the log-transformed data (see Figure 9a). Therefore the discharge rate normalized by the lake area includes the least bias generated by the different geometrical settings for the lakes we compared, and allows for a comparison of lakes with different areas.

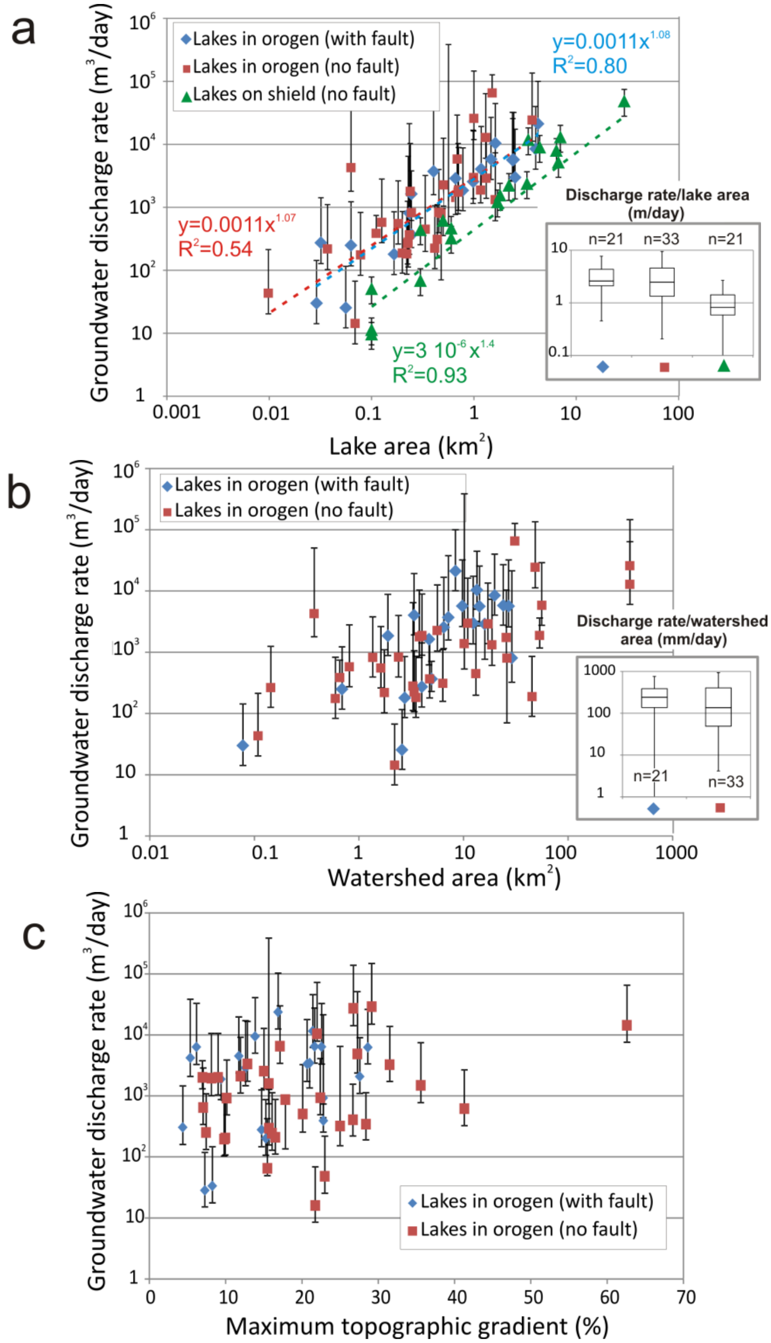

Figure 9 - The groundwater discharge rates estimated through the steady-state model are plotted for the two categories of lakes (fault or no fault) versus (a) the lake area, (b) the watershed area, and (c) the maximum topographic gradient. Data from Gleeson (2009) are also represented in the first graph (lakes on shield). The orogen is an Appalachian mix of volcanic and sedimentary rocks whereas the shield refers to the Canadian Shield with crystalline rocks. The distribution of the ratio of the groundwater discharge rates to the lakes areas (a) and to the watershed areas (b) are also represented with a boxplot.

iii. Sensitivity analysis

The sensitivity of the steady-state model to its various input parameters (lake area and depth, evaporation, precipitation and gas exchange rate, and the chloride concentration and radon activity in the lake, the surface water inflow, the groundwater inflow, and the precipitation) was determined using two approaches (Figure 10). First, we carried out the sensitivity analysis on a “typical” lake, for which the lake parameters were estimated taking the mean of the values measured for all the lakes. Figure 10a shows the calculated discharge rate when varying continuously the 12 parameters sequentially from 50 to 150% of their measured mean or assumed value. The two first graphs which represent the changes in discharge rate while varying the chloride concentration in lake and in surface inflow show unexpected patterns as the model actually diverges for a certain range of values. The divergence occurs when the difference between the two values of surface chloride concentration ($C_{S,Cl}$ and C_{Cl}) tends to zero. The calculation of the discharge rate in our model is indeed based on the difference between the differences of chemical activities in surface inflow and in the lakes. Therefore, the estimation of the discharge rate is biased for a range of values for $C_{S,Cl}$ and C_{Cl}, when their difference is too small to enable the differentiation between water from the surface inflow from the lake water. Away from the anomaly, the discharge rate is stable though and is not very sensitive to chloride concentrations. Therefore, our results are not much affected by the model instability as long as we make sure that the values of both parameters lie outside of the critical interval. This will be discussed further below in the Monte Carlo analysis. For the other parameters, the variation is monotonic, and insignificant except for the radon activity in groundwater, in the lake and the gas exchange rate and the lake depth.

Second, we assessed the global sensitivity, calculating the mean discharge rates for all the lakes while varying the input parameters, and averaging the observed variations (Figure 10b). Every parameter was varied sequentially by respectively ±20% and ±50% and the averages of the calculated discharge rates for the 54 lakes were plotted for each variable. The most sensitive variable is the radon activity in groundwater. A change of 50% in the radon activity in groundwater leads to a change of 120% in the averaged discharge rate, giving this parameter a crucial role that will be discussed below. The model is not sensitive to the evaporation and precipitation rates, chloride concentrations in groundwater, in precipitation, and in surface water and lake area. However, it is moderately sensitive to lake radon activity, lake depth and the gas exchange rate. The gas exchange rate carries an important uncertainty, as it was not directly measured but rather assumed by a value computed by Cook et al (2008) in small wetlands. However, since the variation with the gas exchange rate is linear, as it is shown in Figure 10a, and should be the same for all the lakes since all the lakes are in the same area and within a similar environment, an incorrect estimation of the gas exchange rate will offset all the results in the same way, and will not affect the comparison between the lakes located on a fault zone and those away from a fault zone.

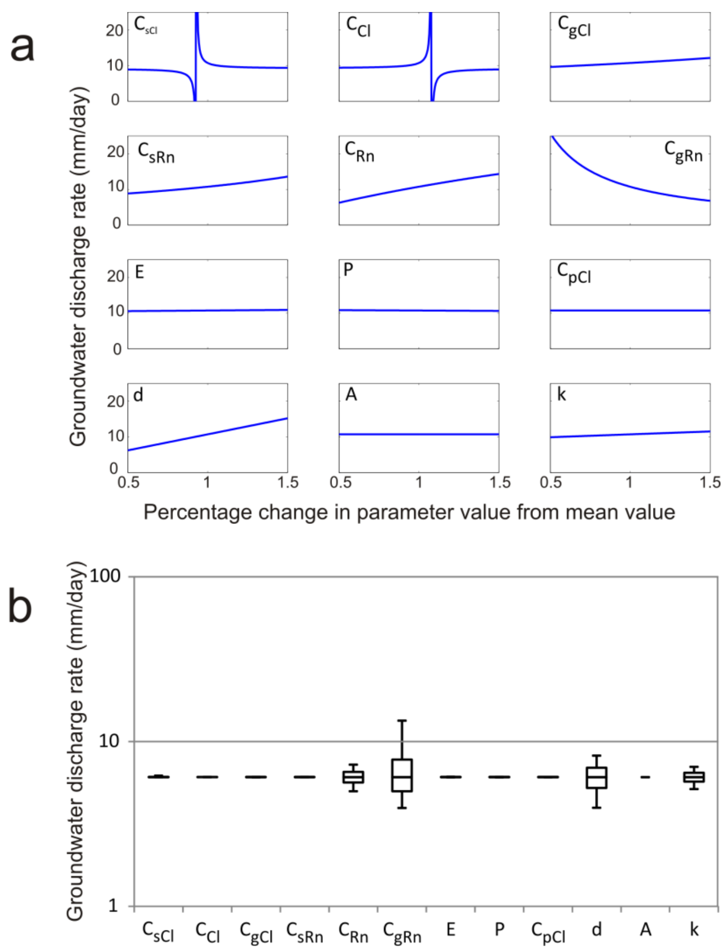

Figure 10: Sensitivity analysis to the model parameters, in order: chloride concentration in surface inflow (C_{sCl}), in lake (C_{Cl}), in groundwater (C_{gCl}), radon activity in surface inflow (C_{sRn}), in lake (C_{Rn}) and in groundwater (C_{gRn}), evaporation rate (E), precipitation rate (P), chloride concentration in precipitation (C_{pCl}), lake depth (d), lake area (A), and gas exchange rate (k). Each parameter is varied over a range of ±50%. In (a), the steady-state model was applied to a fictive typical lake to which we assigned average values for concentrations and dimensions. The curve represents the variation of the calculated discharge rate while varying one of the parameter from -50% (0.5) to 50% (1.5). In (b) the discharge rate was calculated for all the lakes and the average value is represented. The rectangles correspond to ±20% of variation whereas the error bars correspond to variations of 50%. The horizontal lines in the middle of the rectangles are the mean discharge rates calculated with the original values attributed to each parameter.

Because the radon activity in groundwater is a critical parameter, the sensitivity of our model to groundwater radon activity was investigated further over more detail using a Monte Carlo method. The discharge model was run 5,000 times, considering the radon activity in groundwater as a random variable, following the observed distribution, which is a lognormal distribution (see Figure 11), with a mean equal to the previously estimated value and a standard deviation of 80% of the mean. Figure 12 shows the results of the Monte Carlo simulation for each lake. The difference between the median discharge rates of the Monte Carlo simulation and the previously estimated discharge rates are emphasized by filling the rectangle with red. The average difference between the median of the Monte Carlo simulation and the value previously estimated with the analytical model is 12%. The median discharge rates are equal to the results of the former estimations with less than 20% error for all the lakes but three. However, for these three lakes (numbered 23, 24 and 48 in Table A.1 and A.2), the value assigned to radon activity in groundwater greatly changes the calculated groundwater discharge rate. Therefore for these three lakes, our estimation from the steady-state model includes a high error, due to the uncertainty in the value of radon activity in groundwater. Nevertheless, the error caused by the uncertainty in groundwater radon activity is acceptable for the other 51 lakes.

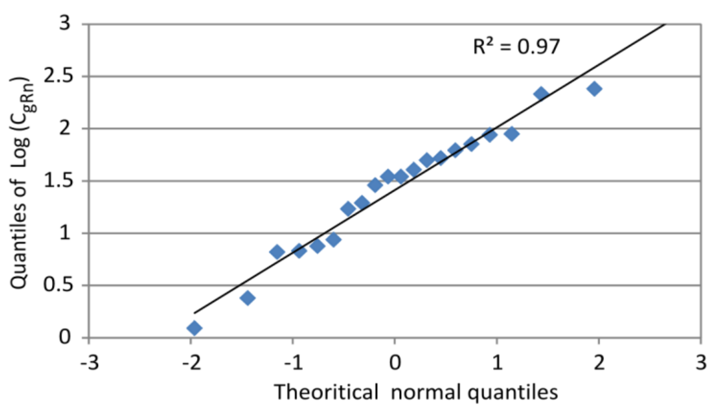

Figure 11: The logarithm of the radon activities in the 20 groundwater samples is plotted versus their normal z-scores. A high correlation coefficient for a linear regression shows that the data is lognormal.

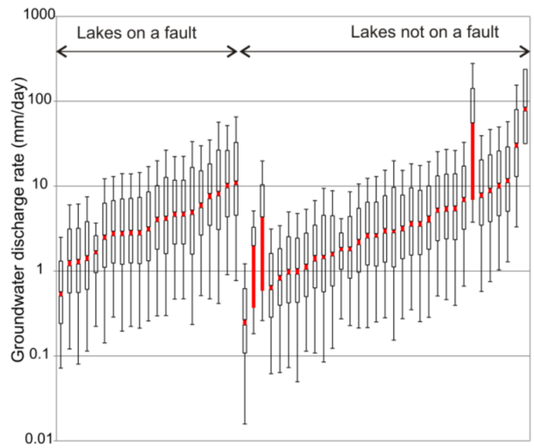

Figure 12: Results of Monte Carlo analysis for the uncertainty in radon activity in groundwater. The rectangles include 90% of the values obtained, between the $1/10^{th}$ and the $9/10^{th}$ quantile. The error bars represent the minimum and maximum values after removing the extreme outliers, defined as the values outside of three interquartile ranges from each side of the box. The red-filled rectangles represent the difference between the discharge rate previously estimated and the median of the values obtained with the Monte Carlo simulation. Three lakes show high deviation, whereas for the 51 remaining lakes, the difference between both values is less than 20%.

The impact of the cumulative uncertainties on the discharge rates was also assessed with a Monte Carlo method. The model was run for 5,000 realizations considering all the parameters as random variables following a normal distribution with a mean equal to our estimations of the parameters and a standard deviation of 20% of the mean. The results are presented in Figure 13. The histograms of the results of the Monte Carlo simulation for each lake are represented on the left. The narrower the peak, the smaller the uncertainty in our model. The discharge rates estimated with the original values for all parameters are also represented for each histogram with a red line, as well as the median discharge rate calculated with the Monte Carlo results with a black line. When both lines do not coincide, the error in the model is large, and the previously estimated values are probably biased. For seven lakes (numbered 16, 21, 23, 26, 31, 33, 34, 39), both values show more than 10% difference, suggesting that the discharge rate calculated with the measured values is less reliable. However, for the remaining 47 lakes, the differences between the mean discharge rates of the 5,000 realizations and the model estimated discharge rate is less than 10%, and the standard deviation of the 5,000 realizations are within 60% of the mean discharge rates.

Figure 13c and d explain the variability of the calculated discharge rates. The curves show how the discharge rate varies with chloride concentration in the lake, in the surface inflow and the radon activity in the lake and in groundwater varying from -50% to +50% of the measured value. For 16 lakes, chloride concentration cause instability, and that situation corresponds to the lakes where chloride concentrations measured in surface inflow and in the lake are close. When the peaks are near the middle of the graph, the measured chloride concentrations lay in the critical range, and the estimations of the discharge rates from the original measures could be biased. This is the case for the seven above mentioned lakes, explaining why the previously estimated value is different from the median values of the Monte Carlo results. However, the sensitivity to chloride concentrations in both water bodies is insignificant away from the critical zone, and the estimation of the discharge rate changes by less than 1% when the value of chloride concentration changes by 50%. Then, for the seven lakes that show a larger uncertainty, the estimation through Monte Carlo method is therefore more reliable as it corresponds to non-critical values for chloride concentrations. Therefore, the discharge rates analyzed in the following statistical analysis are the median values calculated from the Monte Carlo simulation.

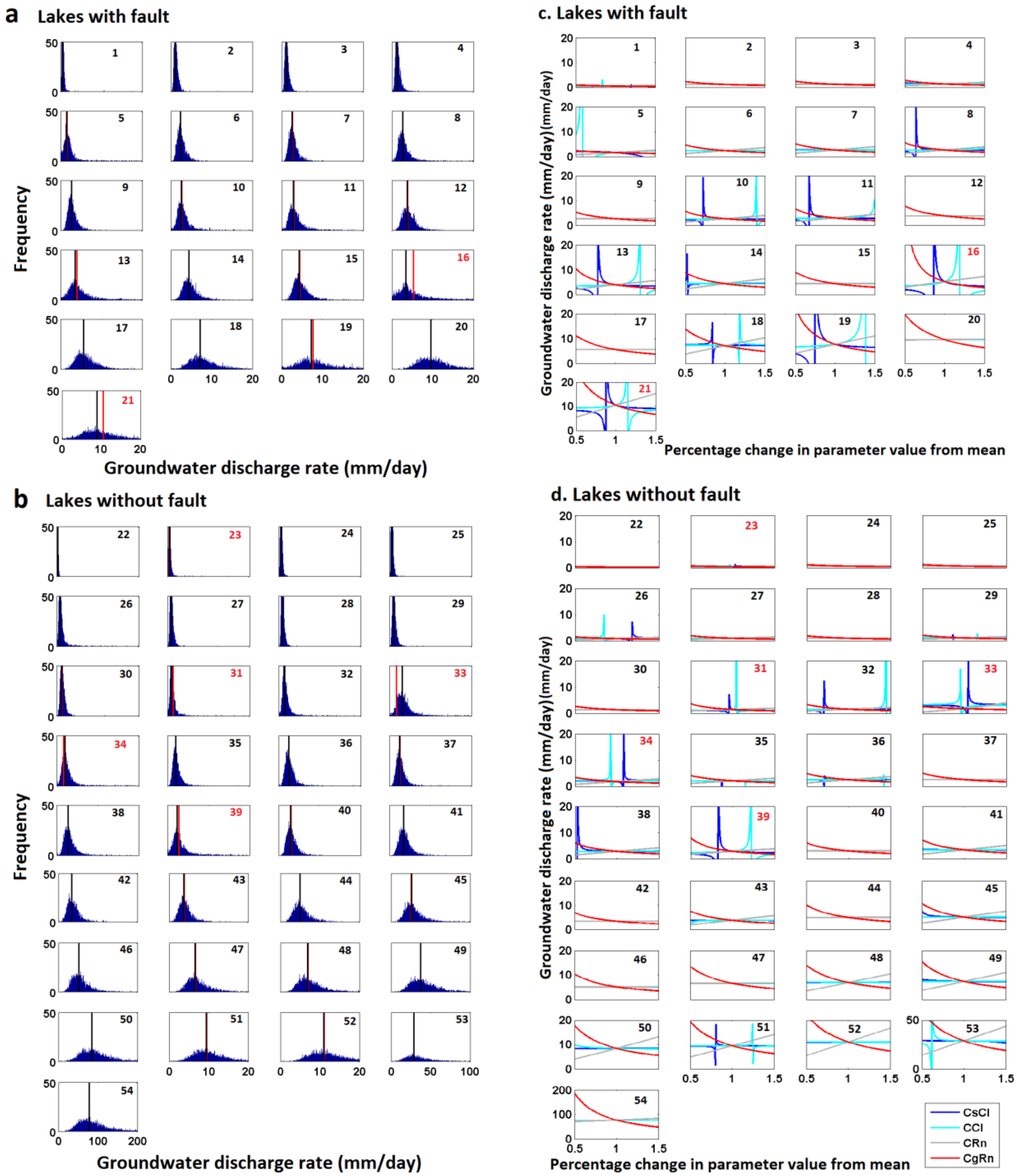

Figure 13: The results of Monte Carlo simulation are represented with histograms for the lakes with fault (a) and the lakes without fault (b).The vertical black line represents the median discharge rate of Monte Carlo results, whereas the red line represents the previously estimated discharge rate. When both lines do not overlap (numbers in red), there is a significant difference between the estimated discharges from both methods. In (c) and (d), the sensitivity of the model to four parameters (chloride concentrations and radon activities in surface inflow and in the lakes) is represented for each lake. The four parameters are varied sequentially by ±50%.

iv. Statistical analysis

We used statistical analysis to test the above qualitative assessment suggesting that there is no difference in the groundwater discharge rate for lakes located on a fault and the others. We sequentially compared pairs of discharge rates from the three populations: lakes in the Appalachian orogeny with fault zones, lakes in the Appalachian orogeny without fault zones and lakes on the crystalline bedrock of the Canadian Shield. The three data sets are log-normal (Figure 14). Therefore we apply both the Welch t-test and the Kolmogorov-Smirnov test to the paired log-transformed data-sets.

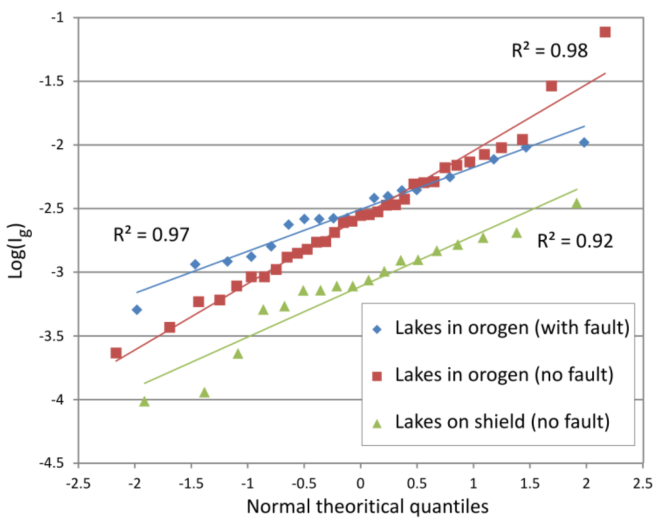

Figure 14: Lognormal Q-Q plot for the calculated groundwater discharge rates. High correlation coefficients mean that the data is lognormal.

First, when comparing the lakes from the Appalachians overlying a fault zone and the ones from the Appalachians not overlying a fault zone, the null hypothesis stipulating that both populations have the same mean is rejected for none of the statistics tests (Table 3). The values of the t-statistics, which illustrates the difference between the two groups, are low, suggesting that we cannot differentiate the groups of lakes with our data. The p-values of both tests are high (60% and 48% for respectively the Welch t-test and the Kolmogorov-Smirnov test), confirming that with our results, we cannot determine a statistically significant difference in the groundwater discharge rates for the lakes located on a fault and the lakes not underlain by a fault zone. Comparing both populations to the discharge rates calculated in the Canadian Shield with the two tests indicates that the Appalachian lakes are different than the Canadian Shield lakes with a high significance, since the p-values are much smaller than the confidence level of 5%.

A second computation was carried out on the discharge rates for the 47 lakes that were robust based on the Monte Carlo simulation for cumulative uncertainty. When comparing the Appalachian lakes overlying or not a fault zone, the null hypothesis cannot be rejected for both Welch and Kolmogorov-Smirnov tests, and the p-values are even higher than in the computation with all the lakes. When comparing both groups of lakes in the Appalachian orogen to the lakes in the Canadian Shield, the null hypothesis is rejected for both tests with high confidence, since the p-values are much below the confidence level of 5%.

There is therefore no significant difference between the calculated discharge rates for the lakes located on a fault and the lakes that do not overlie a fault located in the Appalachians. However the lakes located in the Canadian Shield and the lakes located in the Appalachians have a significantly different groundwater discharge independent of whether they are located on a fault zone or not. Therefore, fault zones do not significantly affect groundwater discharge rates.

Table 3: Statistics results with bold indicating that the null hypothesis was rejected

			Fault (orogen) *v.s.* No fault (orogen)	Fault (orogen) *v.s.* No fault (shield)	No Fault (orogen) *v.s.* No fault (shield)
54 lakes	Welch – test	*t-stat*	*0.53*	***5***	***4.1***
		p-value	0.60	**1.9×10^{-5}**	**2×10^{-4}**
	Ks - test	*t-stat*	*0.48*	***5.08***	***3.79***
		p-value	0.63	**1×10^{-5}**	**4×10^{-4}**
47 lakes	Welch – test	*t-stat*	*0.2*	***4.9***	***4.1***
		p-value	0.85	**2×10^{-5}**	**1.6×10^{-4}**
	Ks - test	*t-stat*	*0.17*	***0.69***	***0.61***
		p-value	0.85	**8.3×10^{-5}**	**2.9×10^{-4}**

The robustness of the two statistics tests regarding the uncertainty of the radon activity in groundwater was assessed using the Monte Carlo analysis described above. We calculated both statistics tests for each run of the Monte Carlo simulation (Table 4). The p-values are indicated, as well as the frequency of rejection of the null hypothesis for the Monte Carlo simulations. The comparisons between the data sets from the Appalachians and the data set from the Canadian Shield lead systematically to the rejection of the hypothesis, corroborating the previous conclusion that the groundwater discharge rates in the Appalachian orogen are greater than the groundwater discharge rates in the Canadian Shield. When comparing the groundwater discharge rates to the lakes in orogen located on a fault zone to the groundwater discharge rates to the lakes in orogen not overlying a fault, the null hypothesis is rarely rejected, and the averaged p-values are still high for both tests.

In sum, whereas the discharge rates estimated in the Appalachian region are significantly different from the discharge rates estimated in the Canadian Shield, there is no significant difference between the discharge rates of groundwater to lakes with underlying faults and to lakes that do not have underlying faults in the Appalachian region.

Table 4: Statistics results for the Monte Carlo simulations with bold indicating the rejection of the null hypothesis

			Fault (orogen) *v.s.* No fault (orogen)	Fault (orogen) *v.s.* No fault (shield)	No Fault (orogen) *v.s.* No fault (shield)
54 lakes	Welch –test	# of rejection	**4**	**5000**	**5000**
		p-value (mean)	0.65	**8.2×10^{-9}**	**6.8×10^{-9}**
	Ks – test	# of rejection	**38**	**5000**	**5000**
		p-value (mean)	0.61	**2×10^{-7}**	**5.1×10^{-8}**
47 lakes	Welch – test	# of rejection	**36**	**5000**	**5000**
		p-value (mean)	0.56	**7.7×10^{-9}**	**9..9x10^{-9}**
	Ks – test	# of rejection	**56**	**5000**	**5000**
		p-value (mean)	0.59	**2.4×10^{-7}**	**2.9×10^{-7}**

v. Model uncertainty

Our analytical steady-state model includes numerous assumptions. First, the radon budget did not consider radon contribution from sediments diffusive flux. Because the groundwater discharge rates calculated were high (up to 50,000 m^3/day), the radon contribution mainly comes from the groundwater flow. Cook et al (2008) calculated the radon diffusive flux into a shallow wetland in Australia, and gives a maximum estimation of 10 Bq/m^2/day. We can compare this value to the radon flux that comes from groundwater discharge. The median discharge calculated in our analysis is 2.8 L/m^2/day (2.8 mm/day). Since the radon activity in groundwater is estimated as 34.5 Bq/L, the groundwater radon flux is equal to 95 Bq/m^2/day, which is almost one order of magnitude higher than the radon diffusive flux from sediments. However, for the lakes with the smallest discharge

(0.2 and 0.3 mm/day), the radon flux from groundwater flow is comparable to the radon diffusion flux, therefore the discharge rate may be overestimated.

Therefore, the hypothesis of the lakes being well mixed can be questioned, especially for small lakes where water circulation can be limited and radon activity may not be homogeneous. Because of the cost of radon analysis, only one sample was taken from most lakes, so that this hypothesis could not be verified. However two lakes were sampled at two different locations, as control testing, and both samples showed similar radon activity as well as chloride concentration with less than 20% error (Table 5). Moreover, only one lake is smaller than 10,000 m^2, so that the hypothesis of well mixing seems reasonable.

Table 5: Radon activity at two different locations for two lakes that were sampled twice

	Lake area (km^2)	*Chloride concentration (mg/L)*			*Radon activity (Bq/L)*		
		Location 1	**Location 2**	**Difference**	**Location 1**	**Location 2**	**Difference**
Lac Brais	0.24	1.1	1.2	8.5%	0.011	0.012	8.5%
Lac Breeches	2.5	2.1	1.8	15%	0.038	0.04	4%

We also considered that chloride could only come from precipitation, groundwater and/or surface water inflows. However chloride can be derived from numerous anthropogenic activities such as road salt, and there is a non-negligible uncertainty on the chloride contribution in our model. Moreover, the sensitivity analysis showed that chloride concentrations in surface inflows and in lakes can be critical parameters that cause the divergence of the model. In order to address the uncertainty due to unknown sources of chloride, we computed the groundwater discharge rates with the steady state model using bromide instead of chloride. Bromide is found in much lower concentrations than chloride, but it was detectable for all the lakes but six, so that we could estimate the groundwater discharge rate for 48 lakes. Figure 15 shows the results of the groundwater discharge rates computed with bromide compared to the previous results calculated with chloride. For 44 of the lakes, the estimated discharge rates from both models are the same with an error inferior to 50%. Because of the low concentrations of bromide, the results computed with bromide have higher uncertainty, so that a difference of 50% between the two calculations is acceptable, and does not question the results estimated with chloride. Moreover, if we run the statistics tests on the 44 robust results from the bromide model, we observe the same result suggesting that the groundwater discharge rates are not significantly different in presence or in absence of a fault zone (Table 6).

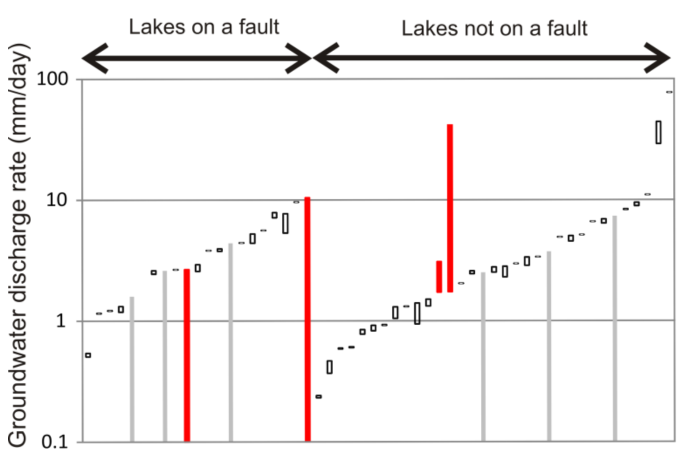

Figure 15: Comparison with the model computed with bromide instead of chloride. The rectangles represent the differences between the discharge rates estimated with chloride and the ones estimated with bromide. The grey data represent lakes where bromide was not detected, so that the comparison is not possible. The red data represent the data that show more than 50% difference between the two calculations. For the other lakes, the results are quite similar, suggesting the chloride values measured give consistent results.

Table 6: Results of statistics tests for the discharge rates calculated with the steady-state model using bromide instead of chloride

			Fault (orogen) *v.s.* No fault (orogen)	Fault (orogen) *v.s.* No fault (shield)	No Fault (orogen) *v.s.* No fault (shield)
44 lakes	Welch – test	*t-stat*	*0.28*	***4.4***	***3.7***
		p-value	0.78	**1.0×10^{-4}**	**6.7×10^{-4}**
	Ks - test	*t-stat*	*0.22*	***0.69***	***0.52***
		p-value	0.63	**2.3×10^{-4}**	**0.0034**

Also we considered a steady state model where the lakes water levels are constant. Since radon residence time in the lakes is shorter than a week the time scale of our steady state model is about a week. Therefore, considering that there is no large change in water level within one week is reasonable. However we tested the sensitivity of our steady state model to a change in the lake water level of ±50 mm/day. (Figure 16) This value was derived from the data on water level for one of the lakes of our study, and was chosen as the maximum of the observed daily variations (Figure 17). For 41 lakes, the results are consistent and the changes in water level do not affect the discharge rate by more than 50% (data in black). Therefore the approximation of steady-state is acceptable for these 41 lakes. However, for the seven critical lakes from the Monte Carlo simulation for cumulative uncertainties (in red), as well as for 6 more lakes (in grey) the changes in water level highly affect the estimation of the discharge rate, and the results show more than 50% difference with the scenario with a steady-state water level. The estimations of discharge rates for these 13 lakes probably contain a small bias due to the hypothesis of steady-state. However, sampling in low-flow conditions, we minimized the variability in water level, and a variation of 50 mm within a day is not likely to happen so that the potential change in discharge rates due to this assumption is overestimated. Nevertheless, if we run the statistics tests on the 41 robust lakes, the results remain the same, and no significant difference is noticeable between the lakes located on a fault zones and the other lakes (Table 7). We believe that the variability caused by the hypothesis of a steady-state condition does not change our main result suggesting that fault zones do not significantly impact groundwater flow, although the estimation of the discharge rates can include a small bias. Therefore, even if the estimation of the groundwater discharge rates still shows high uncertainty for 13 lakes of our study, the final result is robust, confirming that there is no significant difference in the groundwater discharge rates in presence or absence of a shallow fault zone.

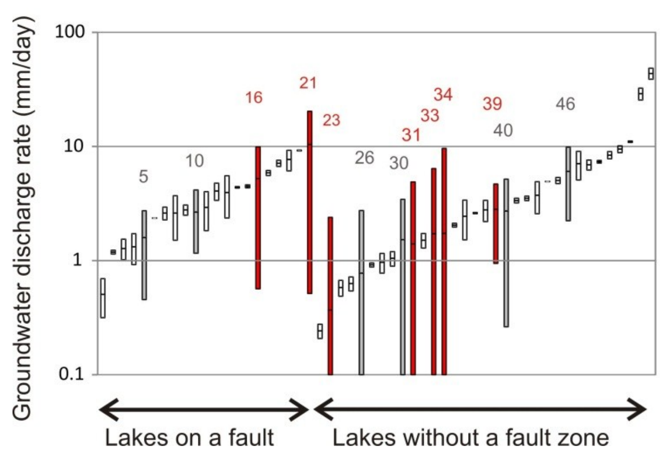

Figure 16: Estimation of the groundwater discharge rate for each of the 47 lakes when the lake is not at a steady state. Extremities of the rectangles show the value corresponding to a change of + or - 50 mm/day. The red data represents the lakes that showed a high variability with the Monte Carlo method for cumulative uncertainty, whereas the grey data represents the lakes that show a high variability only for this analysis. The highly variable lakes with Monte Carlo method also show a high variability to the water level. The black data show lakes that present a low variability, so the estimation of the groundwater discharge rate is robust for these lakes.

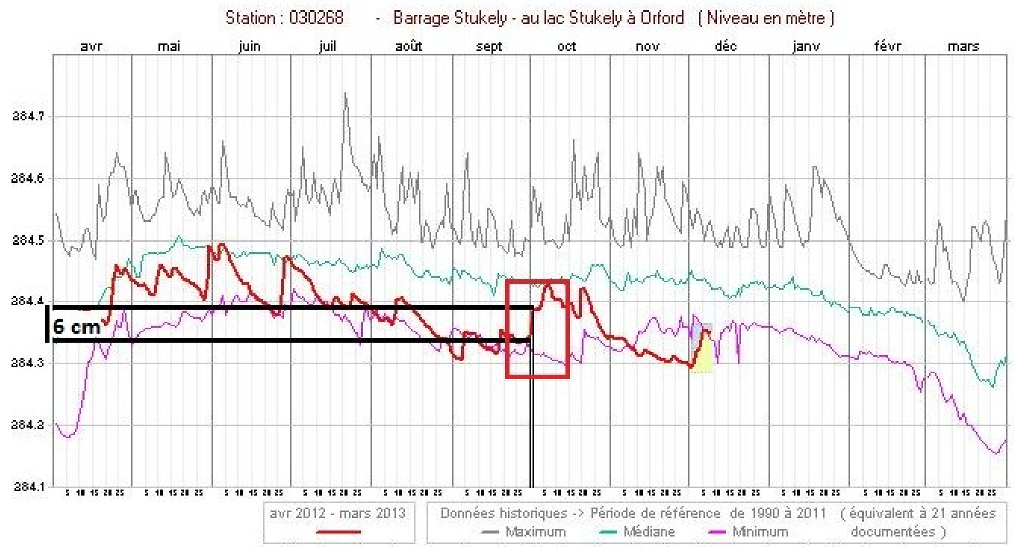

Figure 17: Water level over a year for Lake Stukely. The red curve indicates the changes in water level observed in 2012. The maximum slope over the Fall (our sampling season) is shown in the red box and corresponds to an increase of 6 cm, over ~1.25 days, which corresponds to ~50mm/day.

Table 7: Results of statistics tests for the 41 lakes robust regarding the steady-state hypothesis

			Fault (orogen) *v.s.* No fault (orogen)	Fault (orogen) *v.s.* No fault (shield)	No Fault (orogen) *v.s.* No fault (shield)
41 lakes	Welch – test	*t-stat*	*0.33*	***4.6***	***4.2***
		p-value	0.74	**6.1×10^{-5}**	**1.5×10^{-4}**
	Ks - test	*t-stat*	*0.19*	***0.71***	***0.61***
		p-value	0.82	**1.2×10^{-4}**	**4.3×10^{-4}**

b. Numerical model

Flow simulations were carried out to estimate the impact of fault zones on groundwater flow. First the impact of the fault zone permeability structure on the groundwater flow was studied, comparing the groundwater flow lines in the base case (no fault) with the three cases corresponding to the three types of fault zone permeability structures (barrier, vertical conduit and distributed conduit).

Therefore, we tested various geometric settings, such as the lake area, upgradient recharge area, and topography in order to better explain the trends we observed in our field analysis. In the 2-D domain, discharge rates are expressed in m^2/day, and the areas are expressed in meters, as a 1-D length. For example, the upgradient recharge area is expressed as the length of recharge zone (m) and is a proxy for watershed area.

i. Fault zone permeability structure

First we tested the three fault zone permeability structures on the base case model, represented in Figure 18. The geometric parameters of the reference model have been chosen as average values representative of all the lakes we sampled: the lake is 500 meters wide, the recharge area 1,000 meters long, and the maximum elevation of the recharge area is 200 meters. Figure 19 shows the flow lines for the three fault zone permeability structures, with both a thin fault zone (10 meters) and a thick fault zone (100 meters) as well as for the base case without fault.

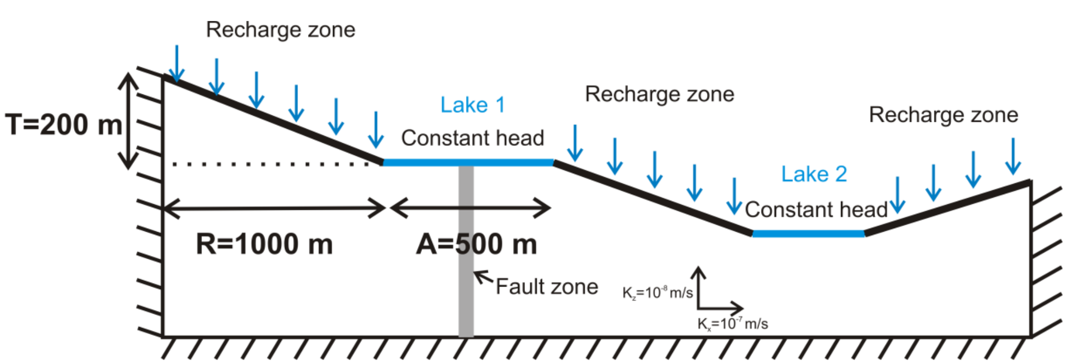

Figure 18: Schematic of the base case model with boundary conditions

The base case configuration without a fault zone generates two flow systems. A local groundwater flow discharges to the first lake and a regional flow system underflows the first lake and discharges to the second lake. The second figure shows the flow lines in presence of a fault zone acting as a barrier to groundwater flow. The fault zone captures a part of the regional flow and channels it toward the first lake. The third figure shows the effect of a barrier fault permeability structure with a 100 m wide fault zone. The local flow is even deeper, but the regional flow still exists. The fourth and fifth figures represent the flow lines for a fault zone acting as a combined vertical conduit and lateral barrier. In that case, the regional flow disappears for both fault zones width, and all the upgradient recharge discharges to the first lake. The two last figures represent the flow lines for a fault zone acting as a distributed conduit. The result is similar to the vertical conduit, with the disappearance of the regional flow and the enhancement of the discharge to the first lake.

Generally, the impact of fault zones on groundwater discharge rate is not significant in our modeling, increasing at the maximum the discharge rate by 11% for a thick fault zone and by 8% for a thin fault zone. The effect of fault zones is more important in the last two configurations where the vertical hydraulic conductivity was increased by two orders of magnitude. And although both settings differ in their lateral hydraulic conductivity they generate very similar flow lines. Hence, in our simulations the vertical hydraulic conductivity of the fault zone controls the groundwater discharge more than does its horizontal hydraulic conductivity.

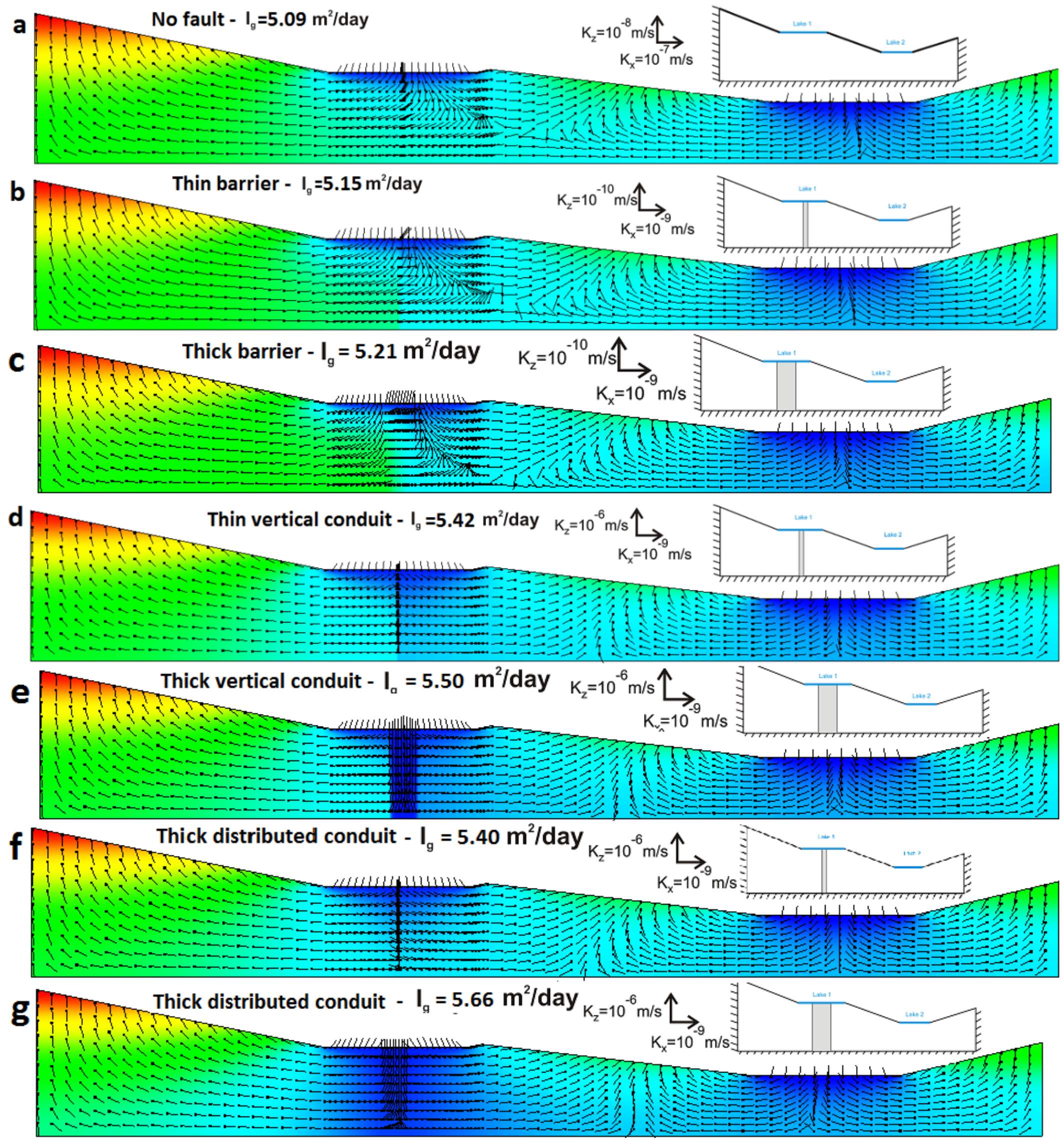

Figure 19: Groundwater flow lines for the base case configuration as well as with the three fault permeability structures, for both thin (10m) and thick (100m) fault zones.

ii. Watershed characteristics

We subsequently tested the influence of the watershed characteristics on the discharge rates and the groundwater flow lines. We simulated various configurations of lake width, the length of the recharge area and its maximum elevation, and computed the groundwater discharge rate to the first lake for each of the three fault zone permeability structures as well as for the case with no fault (Figure 20).

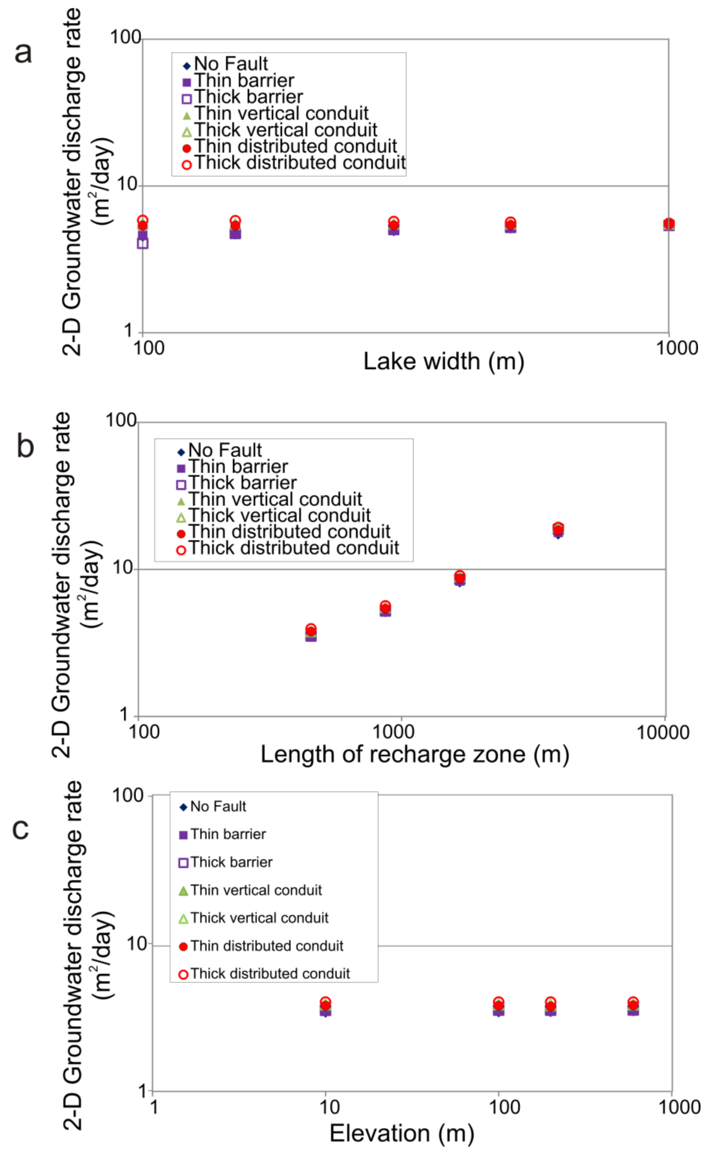

Figure 20: Results of the numerical modeling. Groundwater discharge rates are plotted versus the lake width (a), the length of the recharge zone (b) and the maximum elevation (c), for the configuration without fault, and for the three fault permeability structures, for both thick and thin fault zones.

On Figure 20a, five lake widths were tested, 100 meters, 150 meters, 300 meters, 500 meters and 1,000 meters, while the width of the upgradient recharge area as well as its topographic gradient were kept constant. Without a fault zone, the discharge rate increases with the lake width. However for the two fault zone structures that have a high vertical hydraulic conductivity, the discharge rate slightly decreases when the lake width increases. Increasing the lake's width while the fault zone width is kept constant is equivalent to decreasing the fault zone width while keeping the lake width constant. Then, the discharge is lowered in the case of a larger lake. Also the impact of fault zone is more important for small lakes whereas it is almost not distinguishable for larger lakes. For a 100 meters wide lake underlain by a (thick or thin) fault zone acting as a distributed conduit, the discharge rate is 20% higher than the discharge rate in absence of fault zone.

The difference between Figure 20a and the result from the analytical model on Figure 9a, where the discharge rates are increasing with the lake width is explained by the fact that the recharge area was kept constant in the SUTRA modeling, whereas in reality the size of a lake is related to its associated recharge area. A smaller lake is usually associated with a smaller recharge area (see Figure 21), and therefore has potentially smaller discharge.

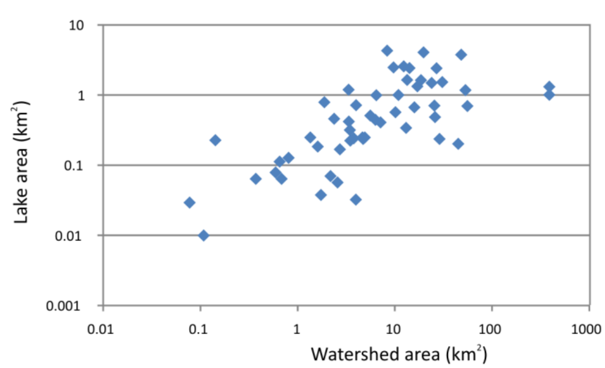

Figure 21: Correlation between the lake areas and their associated watershed areas for the lakes of our study.

Figure A.1 in the Appendix shows the flow lines for two scenarios of lake width (100 and 500 meters) for both cases with or without a fault. When the lake is not underlain by a fault zone, the local system is deeper for larger lake, and the regional flow is then enhanced for smaller lakes. When a lake is underlain by a fault zone that enhances the vertical groundwater flow, the local flow is deep and there is no regional flow system, regardless of the lake's width.

Figure 20b shows the impact of the size of the recharge area on the discharge rate. Four widths of recharge area were tested: 500 meters, 1,000 meters, 2,000 meters and 5,000 meters. The lake width and topographic gradient were kept constant at 500 meters and 0.2, respectively. The larger the recharge area the higher is the groundwater discharge. Larger recharge area results in a larger recharge volume, and naturally a larger discharge. The graph also shows that the recharge area controls groundwater discharge rate much more than does the presence of fault zones. The differences between the three fault zone permeability structures are almost imperceptible in the graph, as compared to the changes due to the size of the recharge area. Flow lines for two scenarios with different widths of recharge area are represented for both cases with or without a fault zone in Figure A.2 in the Appendix. In the absence of a fault zone, the local groundwater flow is deeper for a smaller recharge area. Therefore, although the discharge rate is higher for a larger watershed area, the ratio of discharge to recharge is higher for a smaller watershed area. In the presence of a fault zone, all the values of watershed widths lead to the disappearance of the regional groundwater flow, and again, the ratio of discharge to recharge is higher in the case of a smaller watershed, although the discharge rate is higher.

Figure 20c presents the discharge rates computed with different topographic gradients ranging from 1 to 50%. The graph does not show a significant effect of topography on the discharge rate. The discharge rate is slightly higher when the topographic gradient is higher, but the difference remains less than 1%. Toth (1963) describes the groundwater flow lines depending on the topography and demonstrates that higher relief tends to increase the depth and the intensity of the local groundwater flow system. Figure A.3 in the Appendix shows that the regional flow in slightly reduced for a higher relief, and then the local discharge to the first lake is deeper and more consequent for the lower elevation.

Also the location of the fault zone has a small effect on the discharge rate and the aspect of the flow lines. Figure A.4 shows the flow lines and the corresponding discharge rate for four different positions of the fault zone. The closer the fault is to the recharge area, the smaller the discharge rate, and therefore the lower the effect on the flow lines. The extent of the perturbations of the flow lines downgradient of the lake underlain by the fault is indeed smaller when the fault is further from the downgradient area.

The depth of the aquifer also affects discharge rates, as a deep aquifer enhances the regional and deep groundwater flow. Then, the local discharge rate is smaller for a deeper aquifer. Figure A.5 shows the effect of the aquifer depth on the flow lines for both cases with or without a fault zone acting as a distributed conduit.

For the deep aquifer, the regional flow system is important, even in the presence of a fault zone, and the effect of the fault zone does not appear to be affected by the depth of the aquifer.

In sum, we tested the effect of fault zones on the groundwater discharge rate by modeling groundwater flow in a simple 2-D watershed. The main conclusions are that first, fault zones slightly affect watershed-scale groundwater flow lines and enhance local flow systems. However discharge rates do not change considerably in presence of fault zones as the regional flow that is perturbed is much smaller than the local flow system (Tóth, 1963). Then, in presence of a fault zone, the lake area does not significantly affect the groundwater discharge when the recharge area is kept constant, although the discharge rate increases with the lake area in absence of fault. Finally, the effect of faults is stronger for smaller lakes and watersheds, and becomes imperceptible for larger lakes.

VI. Conclusion

Groundwater discharge rates to 54 lakes underlain by sedimentary and volcanic Paleozoic rocks in eastern Québec have been estimated in order to assess the impact of fault zones on regional groundwater flows. The model used to quantify the groundwater discharge rates combine radon and chloride mass balances, and includes radon and chloride contribution from groundwater and surface water inflow, as well as chloride contribution from precipitation and radon loss through radioactive decay and gas exchange. The results show that there is no significant difference between the groundwater discharge rates in areas overlying fault zones and in areas without fault zones. Hence, although fault zones change the local permeability, shallow fault zones may have no significant impact on the regional groundwater flows in tectonically-inactive sedimentary and volcanic basins.

The simple numerical model we carried out with SUTRA showed that fault zones perturb regional groundwater flow systems and strengthen local flow systems. However the resulting groundwater discharge rates are not significantly impacted by fault zones. Thus, even with a change in hydraulic conductivity by two orders of magnitude for the fault zone as compared to the surrounding bedrock, the groundwater discharge rate to the lake only increases by 11% at the most. While varying the width of the fault zone and its vertical and horizontal hydraulic conductivities, we observed small changes in the groundwater discharge rate. For instance, when the fault zone has a vertical hydraulic conductivity increased by two orders of magnitude, and is 10 meters wide, the change in groundwater discharge rate represents only 8% of the initial discharge rate. In shallow aquifers and with gentle topography, the regional flow rates are indeed much lower than the local flows (Tóth, 1963), so that the perturbation of groundwater flow in presence of fault is difficult to observe. This may then explain why the impact of the fault zones was not visible in our study as it was carried out on small basins including ridge topography with gentle relief.

However the variability of the groundwater discharge rates in our field study is relatively high, with discharge rates ranging from 0.2mm/day to 68mm/day. This distribution could be explained by the differences in watershed characteristics, such as the recharge area, the topography, or even the aquifer geometry, permeability, or geology. For instance, the SUTRA modeling shows that the recharge area, and subsequently the watershed size significantly control the discharge rate more than does the presence of a fault zone. The impact of the differences in the geometry and the geology of the watersheds from the lakes we sampled widely supersedes the impact of the fault zones.

Understanding fault zones impact on regional groundwater systems is a major challenge that can be studied with hydrogeological methods in addition to the structural geology methods. The observation and quantification of groundwater flows around fault zones indeed supplement the available information on the permeability of fault zones, and enable the testing of the model designed by structural geologists. The quantification of groundwater flow using radon forms a very powerful and robust method that can be used to quantify the effects of fault zones on regional groundwater flow in many geological settings.

Because not all the geological settings would lead to the same conclusion that fault zones do not considerably affect regional groundwater flow, we suggest that an integrative approach be used and a data base of fault zones be built, classifying fault zones with their geological characteristics (type of fault, fault architecture, surrounding bedrock) as well as geographical characteristics (watershed dimensions, topography, lakes interconnections), and referencing their impact on regional groundwater flows.

VII. References

2012. Canadian Digital Elevation Data. Canadian Council on Geomatics, GeoBase Canada.

Anderson, L.J., Osborne, R.H., Palmer, D.F., 1983. Cataclastic rocks of the San Gabriel fault - An expression of deformation at deeper crustal levels in the San Andreas fault zones. Tectonophysics 98, 209-251.

Anderson, M.P., 2005. Heat as a ground water tracer. Ground Water 43, 951-968.

Anderson, T.R., Fairley, J.P., 2008. Relating permeability to the structural setting of a fault-controlled hydrothermal system in southeast Oregon, USA. J. Geophys. Res. 113, B05402.

Andrews, J., Burgess, W., Edmunds, W., Kay, R., Lee, D., 1982. The thermal springs of Bath. Nature 298.

Antonelli, M., Aydin, A., 1994. Effect of faulting on fluid flow in porous sandstones: petrophysical properties. American Association of Petroleum Geologists Bulletin 78, 355-377.

Aydin, A., 2000. Fractures, faults, and hydrocarbon entrapment, migration and flow. Marine and Petroleum Geology 17, 797-814.

Barton, C.A., Zoback, M.D., Moos, D., 1995. Fluid flow along potentially active faults in crystalline rock. Geology 23, 683-686.

Bense, V.F., Gleeson, T., Loveless, S., submitted. Fault zone hydrogeology. Earth Sciences Review.

Bense, V.F., Person, M.A., Chaudhary, K., You, Y., Cremer, N., Simon, S., 2008. Thermal anomalies indicate preferential flow along faults in unconsolidated sedimentary aquifers. Geophys. Res. Lett. 35, L24406.

Billi, A., Valle, A., Brilli, M., Faccenna, C., Funiciello, R., 2007. Fracture-controlled fluid circulation and dissolutional weathering in sinkhole-prone carbonate rocks from central Italy. Journal of Structural Geology 29.

Bredehoeft, J.D., 1997. Fault permeability near Yucca Mountain. Water Resour. Res. 33, 2459-2463.

Breesch, L., Swennen, R., Vincent, B., 2009. Fluid flow reconstruction in hanging and footwall carbonates: Compartmentalization by Cenozoic reverse faulting in the Northern Oman Mountains (UAE). Marine and Petroleum Geology 26, 113-128.

Bruhn, R.L., 1993. Crack 2D: An unpublished MatLab computer program for deriving permeability tensors in two dimensions using the methods of Oda, 1986 and Oda et al., 1987.

Bruhn, R.L., Parry, W.T., Yonkee, W.A., Thompson, T., 1994. Fracturing and hydrothermal alteration in normal fault zones. Pure and Applied Geophysics 142, 609-644.

Caine, J.S., Coates, D.R., Timoffeef, N.P., Davis, W.D., 1991a. Hydrogeology of the Northern Shawangunk Mountains, New York State Geological Survey Open-File Report.

Caine, J.S., Coates, D.R., Timoffeef, N.P., Davis, W.D., 1991b. Hydrogeology of the Northern Shawangunk Mountains. New York State Geological Survey Open-File Report 1g806.

Caine, J.S., Evans, J.P., Forster, C.B., 1996. Fault zone architecture and permeability structure. Geology 24, 1025-1028.

Caine, J.S., Minor, S.A., 2009. Structural and geochemical characteristics of faulted sediments and inferences on the role of water in deformation, Rio Grande Rift, New Mexico. Geological Society of America Bulletin 121, 1325-1340.

Cecil, L.D., Green, J.R., 1999. Radon -222, in: Cook, P.a.H., A.L. (Ed.), Environmental tracers in subsurface hydrology. Kluwer Academic Publishers.

Celico, F., Petrella, E., Celico, P., 2006. Hydrogeological behaviour of some fault oznes in a carbonate aquifer of Southern Italy: an experimentally based model. Terra Nova 18.

Chester, F.M., Logan, J.M., 1986. Implications for mechanical properties of brittle faults from observations of the Punchbowl Fault Zone, California. Pure and Applied Geophysics 124, 80-106.

Cook, P.G., Favreau, G., Dighton, J.C., Tickell, S., 2003. Determining natural groundwater influx to a tropical river using radon, chlorofluorocarbons and ionic environmental tracers. J. Hydrol. 277, 74-88.

Cook, P.G., Lamontague, S., Berhane, D., Clark, J.F., 2006. Quantifying groundwater discharge to Cockburn River, Southeastern Australia, using dissolved gas tracers ^{222}Rn and SF^6. Water Resour. Res. 42, doi:10.1029/2006WR004921

Cook, P.G., Wood, C., White, T., Simmons, C.T., Fass, T., Brunner, P., 2008. Groundwater inflow to a shallow, poorly-mixed wetland estimated from a mass balance of radon. J. Hydrol. 354, 213-226.

Dimova, N.T., Burnett, W.C., 2011. Evaluation of groundwater discharge into small lakes based on the temporal distribution of radon-222. Limnology and Oceanography 56 (2), 486-494.

DMTI, 2010. CanMap Water.

Evans, J.P., 1990. Thickness-displacement relationships for fault zones. Journal of Structural Geology 12, 1061-1065.

Evans, J.P., Chester, F.M., 1995. Fluid-rock interaction in faults of the San Andreas system: Inferences from San Gabriel fault rock geochemistry and microstructures. Journal of Geophysical Research 100, 13007-13020.

Evans, J.P., Forster, C.B., Goddard, J.V., 1997. Permeability of fault-related rocks, and the implications for hydraulic structure of fault zones. Journal of Structural Geology 19, 1393-1404.

Fairley, J.P., Hinds, J.J., 2004. Rapid transport pathways for geothermal fluids in an active Great Basin fault zone. Geology 32, 825-828.

Faulkner, D.R., Jackson, C.A.L., Lunn, R.J., Schlische, R.W., Shipton, Z.K., Wibberley, C.A.J., Withjack, M.O., 2010. A review of recent developments concerning the structure, mechanics and fluid flow properties of fault zones. Journal of Structural Geology 32, 1557-1575.

Faulkner , D.R., Jackson, C.A.L., Lunn, R.J., Schlische, R.W., Shipton, Z.K., Wibberley, C.A.J., Withjack, M.O., 2010. A review of recent developments concerning the structure, mechanics and fluid flow properties of fault zones. Journal of Structural Geology 32, 1557-1575.

Flint, A.L., Flint, L.E., Kwicklis, E.M., Bodvarsson, G.S., Fabryka-Martin, J.M., 2001. Hydrology of Yucca Mountain. Reviews of Geophysics 39, 447-470.

Folger, P.F., Poeter, E.P., Wanty, R.B., Frishman, D., Day, W., 1996. Controls on ^{222}Rn variations in a fractured crystalline rock aquifer evaluated using aquifer tests and geophysical logging. Ground Water 34, 250-261.

Genereux, D.P., Hemond, H.F., Mulholland, P.J., 1993. Use of radon-222 and calcium as tracers in a three-end-member mixing model for streamflow generation on the west fork of the Walker Branch Watershed. J. Hydrol. 142, 167-211.

Giurgea, V., Rettenmaier, D., Pizzino, L., Unkel, I., Hotxl, H., Forster, A., Quattrocchi, F., 2004. Preliminary hydrogeological interpretation of the Aigion area from the AIG10 borehole data. Tectonics 336.

Gleeson, T., 2009. Groundwater recharge, flow and discharge in a large crystalline watershed, Department of Civil Engineering Published PhD thesis, Queen's University, Kingston, p. 251.

Gleeson, T., Novakowski, K., Cook, P.G., Kyser, T.K., 2009. Constraining groundwater discharge in a large watershed: Integrated isotopic, hydraulic, and thermal data from the Canadian shield. Water Resour. Res. 45, W08402.

Hall, F.R., Boudette, E.L., Olszewski, W.R., 1987. Geologic controls and radon occurrence in New Englad, in: Graves, B. (Ed.), Radon, Radium, and Other Radioactivity in Ground Water. Lewis, Chelsea, Mich., pp. 15-30.

Haneberg, W.C., 1995. Steady state groundwater flow across idealized faults. Water Resour. Res. 31, 1815-1820.

Hayashi, M., Rosenberry, D.O., 2002. Effects of ground water exchange on the hydrology and ecology of surface water. Ground Water 40, 309-316.

Jourde, H.E.A., Flodin, A., Aydin, L.J., Durlofsky, Wen, X.H., 2002. Computing permeability of fault zones in Eolian sandstone from outcrop measurements. Am. Assoc. Pet. Hydro.. Bull 86, 1187-1200.

Kalbus, E., Reinstorf, F., Schirmer, M., 2006. Measuring methods for groundwater-surface water interactions: a review. Hydrology and Earth System Sciences 10, 873-887.

Kluge, T., Ilmberger, J., von Rohden, C., Aeschbach-Hertig, W., 2007. Tracing and quantifying groundwater inflow into lakes using a simple method for radon-222 analysis. Hydrology and Earth System Sciences 11, 1621-1631.

Knipe, R.J., 1993. The influence of fault zone processes and diagenesis on fluid flow, Diagenesis and Basin Development. AAPG Special Volumes, pp. 135-154.

Koledoyem, B.A., Aydin, A., May, E., 2003. A new process-based methodology for analysis of shale smear along normal faults in the Niger Delta. The American Association of Petroleum Geologists.

Lilliefors, H.W., 1967. On the Kolmogorov-Smirnov test for normality with mean and variance unknown. Journal of the American Statistical Association 62, 399-402.

Long, J.C.S., Billaux, D.M., 1987. From field data to fracture network modeling: An example incorporating spatial structure. Water Resour. Res. 23, 1201.

Lunn, R.J., Shipton, Z.K., Bright, A.M., 2008a. How can we improve estimates of bulk fault zone hydraulic properties?, The Internal Structure of Fault Zones: Implication for Mechanical and Fluid-Flow Properties - Special Publication no 299, pp. 231-237.

Lunn, R.J., Willson, J.P., Shipton, Z.K., Moir, H., 2008b. Simulating brittle fault growth from linkage of preexisting structures. Journal of Geophysical Research 113.

Marsaglia, G., Tsang, W., Wang, J., 2003. Evaluating Kolmogorov`s distribution. Journal of Stastical Software 8, 1-4.

Massey, F.J., 1951. The Kolmogorov-Smirnov Test for Goodness of Fit. Journal of the American Statistical Association 46, 68-78.

Mayer, A., May, W., Lukkarila, C., Diehl, J., 2007a. Estimation of fault-zone conductance by calibration of a regional groundwater flow model: Desert Hot Springs, California. Hydrogeology Journal 15.

Mayer, A., May, W., Lukkarila, C., Diehl, J., 2007b. Estimation of fault-zone conductance by calibration of a regional groundwater flow model: Desert Hot Springs, California. Hydrogeology Journal 15.

Medeiros, W., do Nascimento, A., da Silva, F.A., Destro, N., Trio, J.D., 2010. Evidence of hydraulic connectivity across deformation bands from field pumping tests: two examples from Tucano basin, NE Brazil. Journal of Structural Geology 32, 1783-1791.

Miller, L.H., 1956. Table of Percentage Points of Kolmogorov Statistics. Journal of the American Statistical Association 51, 111-121.

Mozley, P.S., Goodwin, L.B., 1995. Patterns of cementation along a Cenozoic normal fault: A record of paleoflow orientations. Geology 23, 539-542.

Oxtobee, J.P.A., Novakowski, K.S., 2002. A field investigation of groundwater/surface water interaction in a fractured bedrock environment. J. Hydrol. 269, 169-193.

Praamsma, T.W., Novakowski, K.S., Kyser, T.K., Hall, K., 2009. Using stable isotope and hydraulic head data to investigate groundwater recharge and discharge in a fractured rock aquifer. J. Hydrol. 366, 35-45.

Prairie, Y., Soucisse, A., 1999. Rapport sur le suivi de la qualité des eaux. RAPPEL.

Rawling, G.C., Goodwin, L.B., Wilson, J.L., 2001. Internal architecture, permeability and hydrologic significance of contrasting fault-zone types. Geology 29, 43-46.

Rugh, D., Burbey, T., 2008. Using saline tracers to evaluate preferential recharge in fractured rocks, Floyd County, Virginia, USA. Hydrogeology Journal 16, 251-262.

Saffer, D.M., Bekins, B.A., Hickman, S., 2003. Topographically driven groundwater flow and the San Andreas heat flow paradox revisited. J. Geophys. Res. 108, 2274.

Seaton, W.J., Burbey, T.J., 2005. Influence of ancient thrust faults on the hydrogeology of the Blue Ridge province. Ground Water 43, 301-313.

Séjourné, S., Malo, M., 2007. Pre-, syn-, and post-imbrication deformation of carbonate slices along the southern Quebec Appalachian front – implications for hydrocarbon exploration. Canadian Journal of Earth Sciences 44, 543-564.

Sibson, R.H., 1977. Fault rocks and fault mechanisms. Journal of the Geological Society 133, 191-213.

Sophocleous, M., 2007. The science and practice of environmental flows and the role of hydrogeologists. Groundwater 45, 393-401.

St-Julien, P., Slivitzsky, A., 1985. Compilation géologique de la région de l'Estrie-Beauce, Rapport MM 85-04. Gouvernement du Québec, Ministère de l'Énergie et des Ressources.

Tóth, J., 1963. A theoretical analysis of groundwater flow in small drainage basins. Journal of Geophysical Research 68, 4795-4812.

Voss, C.I., and Provost, A.M., 2002. SUTRA, A model for saturated-unsaturated variable-density ground-water flow with solute or energy transport. U.S. Geological Survey Water-Resources Investigations Report 02-4231.

Winter, T.C., 1999. Relation of streams, lakes, and wetlands to groundwater flow systems. Hydrogeology Journal 7, 28-45.

Winter, T.C., Harvey, J.W., Franke, O.L., Alley, W.M., 1998. Ground water and surface water: a single resource. U.S. Geological Survey circular 1139, p. 79.

VIII. Appendix

Table A.1: Data for lakes in orogen with fault

		Dept h m	Area km^2	C_{Rn} Bq/L	C_{sRn} Bq/L	C_{Cl} mg/L	C_{sCl} mg/L	Topo	WS km^2	Ig/A mm/d
1	**Lac Leclerc**	1.86	0.06	0.04	0.06	3.75	3.14	10	2.6	0.5
2	**Lac A5**	0.30	0.03	0.19	0.52	0.41	4.90	8	0.1	1.2
3	**Lac des Français**	2.50	0.17	0.07	0.52	1.35	4.90	21	2.7	1.2
4	**Lac Breeches**	5.00	2.53	0.04	0.52	1.73	4.90	21	12.4	1.3
5	**Lac Brais 2**	7.50	0.25	0.06	0.39	0.76	0.57	23	4.9	1.6
6	**Lac Stukely**	13.08	4.01	0.03	0.03	1.70	0.22	20	19.8	2.4
7	**Lac à la Truite 2**	3.31	2.40	0.12	0.32	4.71	0.70	19	14.2	2.6
8	**Lac Bowker**	34.89	2.45	0.01	0.46	4.36	7.02	23	9.8	2.6
9	**Lac de l'Est**	4.70	0.78	0.09	0.52	1.49	4.90	15	1.9	2.7
10	**Lac du Huit**	5.57	2.38	0.07	0.48	5.24	7.40	27	27.0	2.7
11	**Lac Sunday**	8.00	0.98	0.06	0.52	2.95	4.90	29	6.5	2.9
12	**Petit lac Lampton**	4.00	1.18	0.15	0.52	2.69	4.90	7	3.4	3.8
13	**Lac Parker**	3.58	0.23	0.13	0.47	1.60	2.22	9	29.0	3.9
14	**Lac Caribou**	3.00	1.47	0.22	0.18	1.39	2.62	22	24.0	4.4
15	**Lac de la Mine**	1.00	0.06	0.44	0.52	2.61	4.90	17	0.7	4.4
16	**Lac Long Pond**	4.00	0.66	0.11	0.70	1.52	2.01	16	16.0	5.2
17	**Lac Nicolet**	14.00	4.23	0.07	0.52	1.50	4.90	32	8.4	5.6
18	**Lac Fraser**	8.60	1.62	0.15	0.09	2.94	3.46	15	13.4	7.1
19	**Lac Brais**	8.50	0.25	0.12	0.53	1.25	1.87	9	4.7	7.7
20	**Lac A2**	1.00	0.03	0.94	0.52	0.59	4.90	4	4.0	9.6
21	**Lac la Rouche**	7.00	0.40	0.21	1.17	7.79	9.06	28	7.2	10.4

Table A.2: Data for lakes in orogen without a fault zone

		Depth m	Area km^2	C_{Rn} Bq/L	C_{sRn} Bq/L	C_{Cl} mg/L	C_{sCl} mg/L	Topo	WS km^2	Ig/A mm/d
22	**Etang de la Castorie**	0.50	0.07	0.03	0.52	0.22	4.90	22	2.2	0.2
23	**Lac Bromont**	3.00	0.48	0.15	0.39	5.47	5.33	18	26.0	0.4
24	**Lac Gale**	4.00	0.11	0.15	0.52	4.49	0.52	41	0.7	0.6
25	**Lac Rocheux**	1.00	0.42	0.06	0.52	0.56	4.90	5	3.4	0.6
26	**Lac des Sittelles**	3.00	0.44	0.05	0.25	4.05	3.49	14	6.3	0.8
27	**Lac au Canard**	3.00	1.62	0.04	0.52	0.24	4.90	36	18.7	0.9
28	**Lac Bisby**	1.36	0.22	0.08	0.52	1.08	4.90	10	3.5	0.9
29	**Lac des Monts**	3.00	0.20	0.05	0.04	3.25	3.75	15	45.2	1.0
30	**Lac Malaga**	3.81	0.23	0.05	0.52	3.52	4.90	7	0.1	1.3
31	**Lac Bran de Scie**	2.50	0.23	0.06	0.17	3.14	3.31	25	3.3	1.4
32	**Lac à la Truite 1**	2.00	0.34	0.09	0.16	0.60	0.89	22	13.1	1.5
33	**Lac Bolduc**	2.00	1.16	0.21	0.34	2.64	2.57	7	53.5	1.7
34	**Lac Jolicoeur**	3.00	0.23	0.10	0.50	10.94	10.17	12	4.7	1.7
35	**Lac Simoneau**	9.28	0.45	0.04	0.05	3.72	4.28	29	2.4	2.0
36	**Lac Orford**	15.00	1.32	0.03	0.30	18.91	26.73	23	17.1	2.5
37	**Lac Lemay**	6.00	0.08	0.07	0.52	0.24	4.90	21	0.6	2.5
38	**Lac Coulombe**	5.00	0.70	0.08	0.52	2.29	4.90	8	25.7	2.8
39	**Lac aux Grelots**	1.00	0.56	0.22	0.50	1.58	2.03	6	10.2	2.8
40	**Petit Lac Brompton**	6.62	0.71	0.08	0.52	6.52	4.90	12	4.0	3.0
41	**Lac Bécancour**	5.00	0.99	0.10	0.40	1.05	4.05	13	11.0	3.4
42	**Lac Gilbert**	4.00	0.18	0.13	0.52	1.03	4.90	16	1.6	3.4
43	**Lac Desmarais**	5.00	0.25	0.12	0.52	9.63	4.90	27	1.4	3.7
44	**Lac Carmen**	1.00	0.01	0.49	0.52	1.96	4.90	23	0.1	4.9
45	**Lac Nick**	3.50	0.50	0.21	5.22	2.01	2.52	17	5.6	5.0
46	**Lac Miller**	2.00	0.13	0.34	0.52	4.53	4.90	15	0.8	5.1
47	**Lac Sperling**	1.00	0.04	0.66	0.52	5.50	4.90	13	1.8	6.6
48	**Lac Waterloo**	2.50	1.51	2.52	0.31	13.20	3.65	6	31.0	6.9
49	**Lac Elgin**	11.92	3.71	0.10	0.52	1.13	4.90	28	48.5	7.3
50	**Etang Peasley**	2.50	0.24	0.45	0.18	3.17	1.05	7	3.8	8.4
51	**Lac Trousers**	5.00	0.69	0.30	0.41	8.25	10.30	63	56.1	9.5
52	**Lac à la Truite 3**	3.00	1.30	0.53	0.43	11.32	0.19	13	390	11.0
53	**Etang Stater**	1.50	1.00	2.20	0.53	18.56	11.32	17	390	28.9
54	**Lac Carmen 2**	1.50	0.06	5.22	0.52	2.52	4.90	27	0.4	76.9

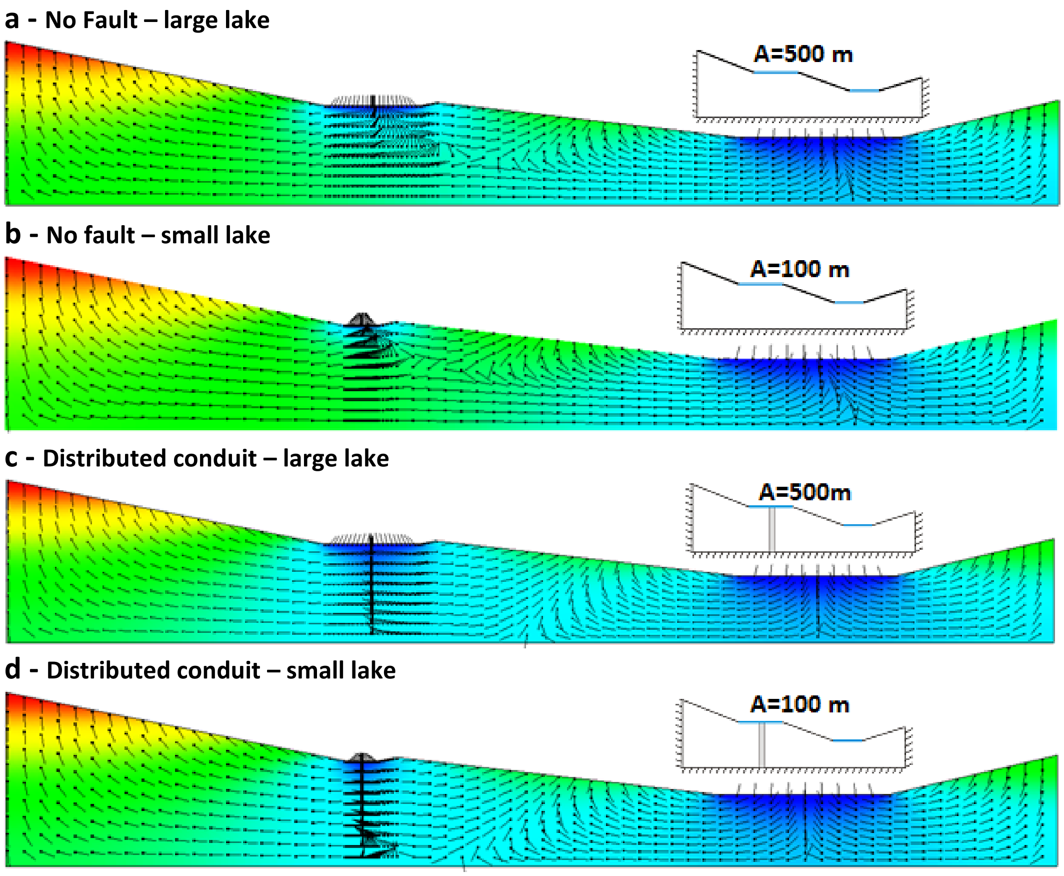

Figure A.1: flow lines for different lakes areas. The effect of a fault zone on the groundwater flow is emphasized for a smaller lake.

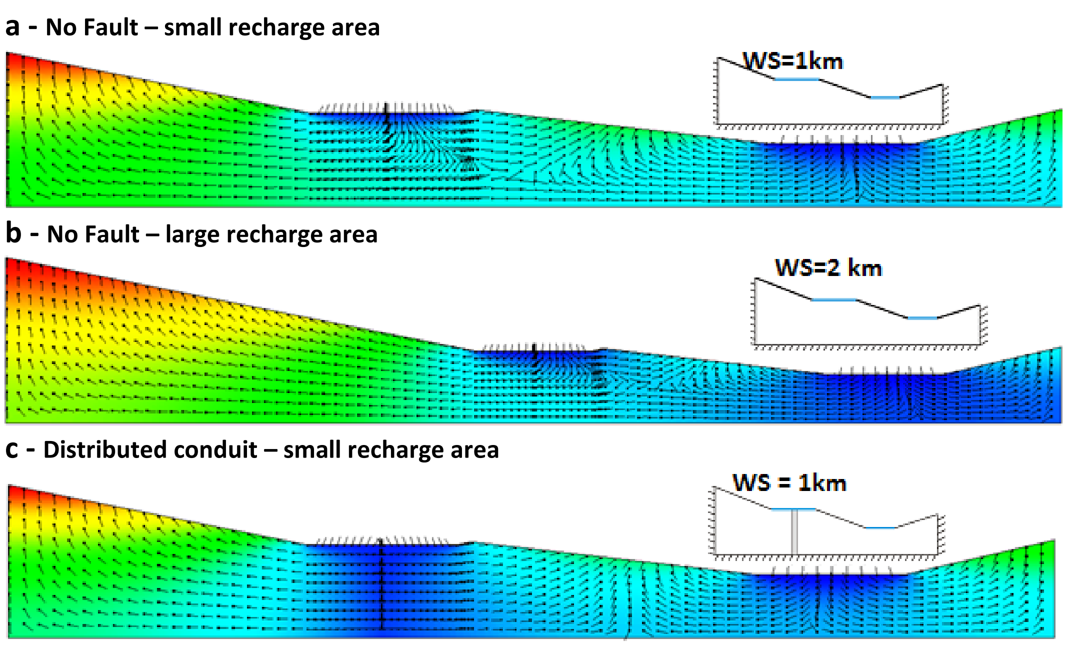

d - Distributed conduit – Large recharge area

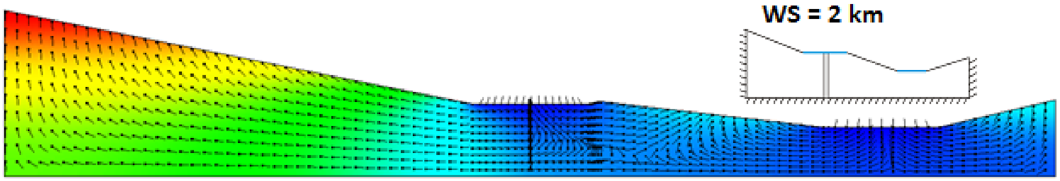

Figure A.2: Flow lines for different length of recharge areas. In smaller watershed, the groundwater flow lines are more perturbed in presence of a fault zone.

a - No Fault – Low topographic gradient

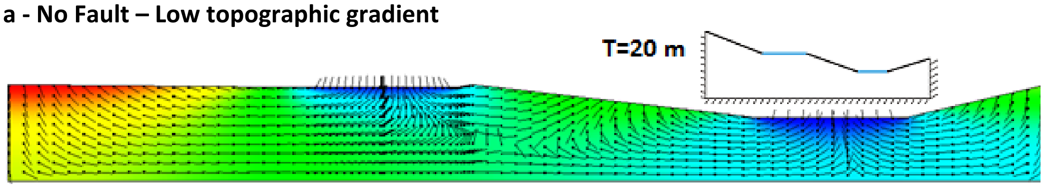

b - No Fault – High topographic gradient

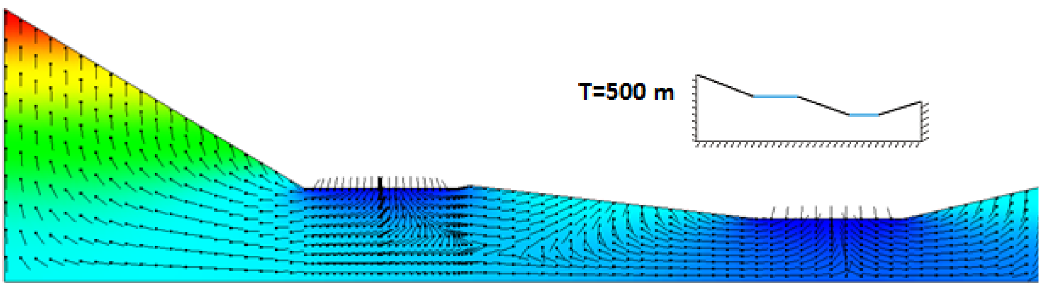

c – Distributed conduit – low topographic gradient

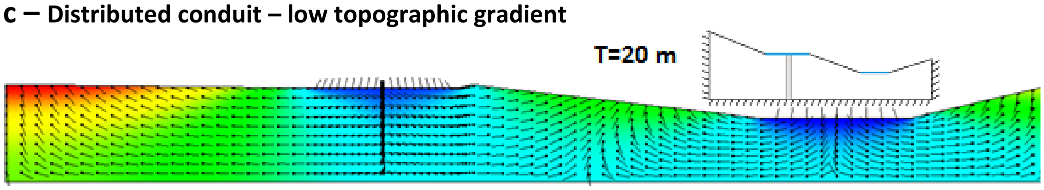

d - Distributed conduit – high topographic gradient

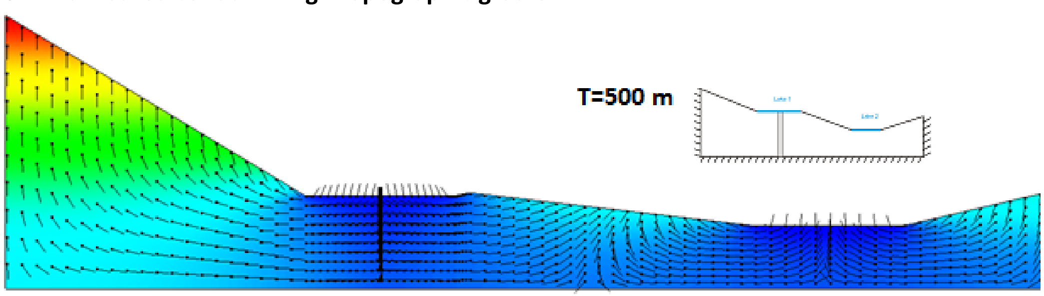

Figure A.3: Flow lines for different topographic gradient. T is the elevation of the highest point, and is a proxy for the topographic gradient.

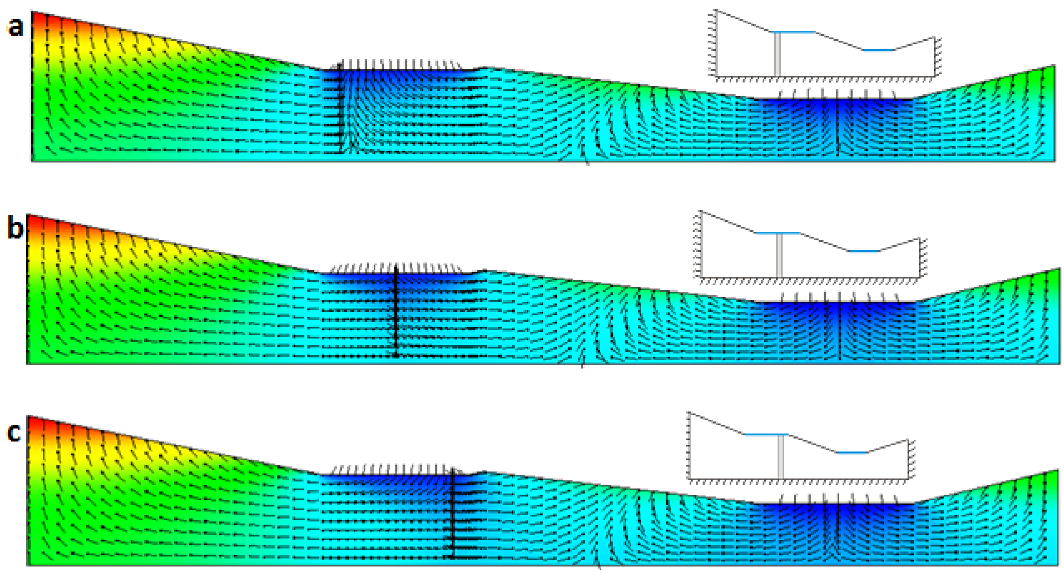

Figure A.4: Flow lines for different location of the fault zone underlying the lake

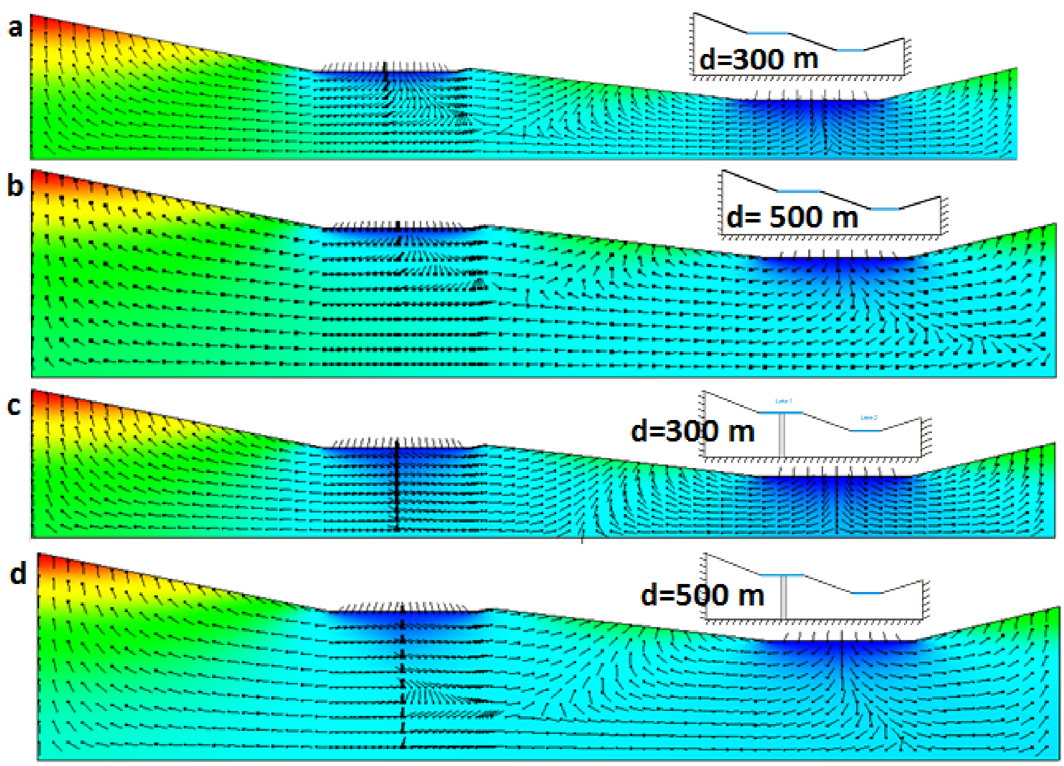

Figure A.5: Comparison between the flow lines in a shallow aquifer (a and c) and in a deeper aquifer (b and d), with or without a fault zone